



HAL
open science

Origin of a core bacterial gene via co-option and detoxification of a phage lysin

Amelia M Randich, David T Kysela, Cécile Morlot, Yves Brun

► To cite this version:

Amelia M Randich, David T Kysela, Cécile Morlot, Yves Brun. Origin of a core bacterial gene via co-option and detoxification of a phage lysin. *Current Biology - CB*, 2019, 29 (10), pp.1634-1646.e6. 10.1016/j.cub.2019.04.032 . hal-02296249

HAL Id: hal-02296249

<https://hal.univ-grenoble-alpes.fr/hal-02296249>

Submitted on 25 Oct 2021

HAL is a multi-disciplinary open access archive for the deposit and dissemination of scientific research documents, whether they are published or not. The documents may come from teaching and research institutions in France or abroad, or from public or private research centers.

L'archive ouverte pluridisciplinaire **HAL**, est destinée au dépôt et à la diffusion de documents scientifiques de niveau recherche, publiés ou non, émanant des établissements d'enseignement et de recherche français ou étrangers, des laboratoires publics ou privés.



Distributed under a Creative Commons Attribution - NonCommercial 4.0 International License

1 **Title**

2 Origin of a Core Bacterial Gene via Co-option and Detoxification of a Phage Lysin

3
4 **Authors**

5 Amelia M. Randich¹, David T. Kysela^{1,2}, Cécile Morlot³, Yves V. Brun^{1,2}

6
7 Correspondence: Y.V.B. yves.brun@umontreal.ca; C.M. cecile.morlot@ibs.fr

8 Lead Contact: Y.V.B. yves.brun@umontreal.ca

9
10 ¹ Department of Biology, Indiana University, 1001 E. 3rd Street, Bloomington, IN 47405 USA

11 ² Faculté de médecine, Département de microbiologie, infectiologie et immunologie, Université
12 de Montréal, Pavillon Roger-Gaudry, 2900, boulevard Édouard-Montpetit, bureau P-607,
13 C.P. 6128, Succursale Centre-ville, Montréal, QC H3C 3J7, Canada

14 ³ Univ. Grenoble Alpes, CNRS, CEA, IBS, 38000 Grenoble, France

15
16 **Summary**

17
18 Temperate phages constitute a potentially beneficial genetic reservoir for bacterial innovation
19 despite being selfish entities encoding an infection cycle inherently at odds with bacterial fitness.
20 These phages integrate their genomes into the bacterial host during infection, donating new, but
21 deleterious, genetic material: the phage genome encodes toxic genes, such as lysins, that kill the
22 bacterium during the phage infection cycle. Remarkably, some bacteria have exploited the
23 destructive properties of phage genes for their own benefit by co-opting them as toxins for
24 functions related to bacterial warfare, virulence, and secretion. However, do toxic phage genes
25 ever become raw material for functional innovation? Here we report on a toxic phage gene
26 whose product has lost its toxicity and has become a domain of a core cellular factor, SpmX,
27 throughout the bacterial order Caulobacterales. Using a combination of phylogenetics,
28 bioinformatics, structural biology, cell biology, and biochemistry, we have investigated the
29 origin and function of SpmX and determined that its occurrence is the result of the detoxification
30 of a phage peptidoglycan hydrolase gene. We show that the retained, attenuated activity of the
31 phage-derived domain plays an important role in proper cell morphology and developmental
32 regulation in representatives of this large bacterial clade. To our knowledge, this is the first
33 observation of a phage gene domestication event in which a toxic phage gene has been co-opted
34 for core cellular function at the root of a large bacterial clade.

35
36 **Keywords**

37 Lysozyme, GH24, Prophage domestication, Bacterial evolution, Alphaproteobacteria,
38 *Caulobacter*, *Asticcacaulis*

39
40 **Introduction**

41
42 Understanding how new genes arise is key to studying the forces that drive diversity and
43 evolution. Although horizontal gene transfer (HGT) is widely regarded as an important
44 mechanism for exchanging *existing* genes among bacteria, mobile genetic elements can transfer
45 exogenous genetic material that gives rise to *novel* genes. These new genes provide the basis for
46 evolving new traits and propelling evolutionary transitions [1,2]. Temperate bacteriophages

47 mediate genetic transfer by integrating their genomes into bacterial hosts [3–6]. These integrated
48 gene tracts, called prophages, remain dormant until induced by various signals to produce phage
49 particles and proteins that lyse the cell. In many cases, prophages contain genes that benefit the
50 host, promoting prophage retention in many bacterial lineages, even after mutations have
51 inactivated the prophage [7–9]. Accumulation of host-specific beneficial mutations in prophages
52 has been referred to as “domestication.” Many domesticated segments of inactivated prophages
53 unexpectedly contain lytic and virion genes, which would intuitively be useless or even
54 detrimental to the bacterial host [7]. Bacteria can use these genes as weapons against competing
55 bacteria and eukaryotic hosts [10–14]. In contrast, we have identified an instance in which a
56 toxic phage gene has not been repurposed as a weapon, but has evolved into a domain in a new
57 core bacterial gene, *spmX*. Here, we report that SpmX resulted from an ancient domestication
58 event at the root of the alphaproteobacterial order Caulobacterales, in which co-option and
59 detoxification of a toxic phage gene gave rise to a novel bacterial gene with roles in
60 developmental regulation and morphogenesis.

61 SpmX was first identified as a developmental regulator in the model organism
62 *Caulobacter crescentus* [15]. Like most members of Caulobacterales, stalked *C. crescentus* cells
63 divide asymmetrically to produce a stalked “mother” cell and a motile, flagellated “daughter” or
64 “swarmer” cell. The *Caulobacter* developmental cycle depends on strict coordination of cell
65 growth, chromosome replication and segregation, and division by various regulatory proteins
66 that differ in localization and timing [16]. This network depends on regulatory phospho-signaling
67 factors localized and regulated by polar scaffolds. SpmX is one protein scaffold that localizes at
68 the stalked pole during the swarmer-to-stalked cell transition and recruits and potentially
69 activates the histidine kinase DivJ [15]. Intriguingly, SpmX is required for stalk synthesis
70 initiation and elongation in the closely related *Asticcacaulis* species *A. excentricus* and *A.*
71 *biprosthicum* [17]. Therefore, this gene appears to have evolved multiple roles for defining cell
72 morphology within this family of dimorphic, stalked bacteria.

73 Perplexingly, SpmX contains an N-terminal phage muramidase domain generally toxic to
74 bacteria. Phages use these enzymatic domains to cleave the bacterial cell wall and lyse bacteria
75 to release infectious phage particles. As a part of SpmX, this domain is critical for SpmX’s role
76 in both developmental regulation and stalk biogenesis: the muramidase domain is necessary for
77 proper SpmX localization in both *C. crescentus* [15,18] and the *Asticcacaulis* genus [17].
78 Various studies have shown that SpmX localizes with the polar scaffold PopZ in *C. crescentus*
79 [19,20] entirely through the muramidase domain [18]. The inability to measure enzymatic
80 activity from purified *C. crescentus* SpmX muramidase domain has led to the conclusion that the
81 domain lost its enzymatic activity and was repurposed for protein interactions and oligomeric
82 assembly [18]. However, given the remarkable sequence similarity of the SpmX muramidase
83 domain to functional phage lysozymes, including the canonical catalytic glutamate, total loss of
84 enzymatic activity seems unlikely. Why would this domain be so highly conserved if its new
85 function were merely for non-essential protein-protein interactions?

86 To better characterize the SpmX muramidase domain and the constraints underlying its
87 conservation, we performed an in-depth bioinformatics study of more than 60 available SpmX
88 genes together with structural determination, biochemical analysis, and comparative cell biology
89 between *Caulobacter* and *Asticcacaulis*. We show that *spmX* arose prior to the diversification of
90 Caulobacterales, a large order of stalked bacteria. We establish that the SpmX muramidase
91 domain is a close relative of GH24 autolysin/endolysins that have been laterally exchanged via
92 prophages. We find that the SpmX muramidase domain exhibits attenuated ancestral phage

93 activity, consistent with its remodeled active cleft. Finally, we demonstrate that this enzymatic
94 activity is necessary for SpmX function in three representative species. We conclude that, close
95 to the time of the genesis of the full-length *spmX* gene, the co-opted muramidase domain
96 accumulated mutations that attenuated its hydrolytic activity on peptidoglycan and detoxified it
97 for bacterial use. To our knowledge, this is the first case of phage gene domestication in which a
98 toxic phage gene has been incorporated into a new core bacterial gene shared by a large bacterial
99 order.

100 Results

101 **The SpmX muramidase domain was co-opted from prophage in an early Caulobacterales**
102 **ancestor.** We first determined the prevalence of SpmX and its homologues in the bacterial
103 domain. Simple pBLAST analysis revealed that SpmX, as defined by its three-part architecture
104 with an N-terminal muramidase domain, a charged and proline-rich intermediate domain, and
105 two C-terminal transmembrane (TM) segments (**Figure 1A**), is taxonomically constrained to
106 Caulobacterales and one member of its sister taxa, Parvularculales. It is conserved as a single-
107 copy gene in all sequenced members (**Table S1**). In all 69 identified *spmX* orthologues, the
108 muramidase domains exhibit high amino acid sequence conservation (**Figure S1**), the
109 intermediate domains high variability in length and sequence conservation, and the TM segments
110 moderate sequence conservation among genera (**Figure 1A**). Apart from these orthologues,
111 BLAST searches using SpmX only returned hits for the muramidase domain. These hits came
112 from Gram-negative bacterial genomes that span the entire bacterial domain and from viral
113 genomes. Most of these bacterial genes are likely to be in prophage regions, as evidenced by
114 their position in tracts of prophage genes. We did not detect sequences homologous to SpmX
115 TMs in our search, although we occasionally detected homologous phage muramidase domains
116 fused to other, non-homologous TM segments.

117 Consistent with finding close SpmX muramidase relatives in prophages, NCBI's
118 Conserved Domain Database (CDD) tool [21,22] clustered SpmX muramidase with glycoside
119 hydrolase 24 (GH24) lysozymes in the autolysin/endolysin class. The sequence cluster diagram
120 in **Figure S2** illustrates the inferred, ancient evolutionary relationships between lysozyme
121 families based on sequence and structural alignments. These relationships allow us to determine
122 a root for the GH24v lysozymes, with SpmX emerging relatively recently within this ancient
123 clade of phage lysozymes. Autolysin/endolysins are closely related to classical phage T4
124 lysozyme-like (T4L-like) peptidoglycan hydrolases, which cleave peptidoglycan and lyse cells
125 during the lytic cycle. These lysozymes are distinct from lytic transglycosylases (**Figure S2**,
126 GH24λ), which include known housekeeping bacterial hydrolases with roles in cell growth and
127 division. Lytic transglycosylases are also assigned to the GH24 group but share no sequence
128 similarity with T4L-like muramidases [23–25]. Thus, although core bacterial genomes encode
129 peptidoglycan hydrolases, the SpmX muramidase domain is most closely related to
130 peptidoglycan hydrolases encoded by prophages and phage genomes.

131 Unlike its close relatives that have been transferred horizontally through the bacterial
132 domain via prophage, the SpmX muramidase domain coding region has been inherited vertically
133 as part of the *spmX* gene in Caulobacterales. The SpmX gene tree mirrors the phylogeny of
134 Caulobacterales from concatenated gene alignments (**Figure 1B**). None of the *spmX* genes
135 appear in tracts of prophage genes. The genomic context of *spmX* appears to be well maintained
136 in members of Caulobacterales, with the gene occurring between a putative Mg²⁺ transporter and
137
138

139 a putative isovaleryl-CoA dehydrogenase in most species. Together, these findings suggest that
 140 SpmX muramidase domain is derived from an autolysin/endolysin no longer within a prophage
 141 island but instead under direct cellular control. It likely fused with the intermediate and TM
 142 domains in a common ancestor of Parvularculales and Caulobacterales. The vertical transmission
 143 of *spmX* and strong sequence conservation of the muramidase domain suggests an important
 144 cellular function for the gene among Caulobacterales members.

146 **The SpmX muramidase domain retains the canonical GH24 motif but contains mutations**
 147 **in the catalytic cleft known to inactivate phage lysozymes.** To determine if critical enzymatic
 148 residues in SpmX muramidase were conserved, we compared SpmX amino acid sequences to
 149 other GH24v lysozymes. By definition, lysozymes catalyze the hydrolysis of β 1,4-linked
 150 glycosidic bonds in peptidoglycan and chitin [25]. This superfamily includes at least seven
 151 distinct groups (five are represented in **Figure S2**) that are unrelated by sequence similarity but
 152 share a common fold in which the catalytic Glu and the beta-hairpin motif in the N-terminal lobe
 153 pack against the C-terminal lobe to form the catalytic cleft (**Figure 2A**) [26]. This beta-hairpin,
 154 or GH motif, contains family-specific residues critical for enzyme activity in all lysozyme
 155 superfamily members [26].

156 We compared the SpmX GH motif to those of lysozymes from the T4L and
 157 endolysin/autolysin classes, which should share the same family-specific residues. **Figure 2B**
 158 shows the amino acid conservation in the GH motif of T4L-like, autolysin/endolysin, closely
 159 related non-SpmX muramidase, and SpmX muramidase protein sequences. Because the
 160 autolysin/endolysin class and the closest non-SpmX relatives are likely to be active phage
 161 enzymes, highly conserved residues shared by these groups with T4L delineate positions that are
 162 evolutionarily constrained for phage lysozyme activity and stability in this clade. For example,
 163 D10 is not conserved outside of T4L-like enzymes because the autolysin/endolysin class does
 164 not have a salt bridge between D10 and the C-terminal lobe [27]. On the other hand, all of the
 165 putative phage sequences (**Figure 2B(i-iii)**) conserve the T4 lysozyme “catalytic triad”: the
 166 catalytic residue E11 and active site residues D20 and T26. While the exact roles of D20 and T26
 167 are not clear, they are critical for effective catalysis [26–29]. Position D20 is very sensitive to
 168 mutation, with only substitutions D20C/A retaining the hydrolytic activity of T4L or P22 phage
 169 lysozymes [30]; these substitutions are tellingly well represented amongst the putative phage
 170 sequences. Remarkably, SpmX muramidase domains demonstrate strong conservation of
 171 residues required for the GH motif, but low conservation of residues associated with catalysis,
 172 with the exception of the main catalytic residue, E11 (**Figure 2B(iv)**). The majority of SpmX
 173 genes contain the mutation D20L/R, both of which reduced T4L activity to less than 3% of WT
 174 in previous studies [27] and which are distinctly unrepresented in the other phage muramidases.
 175 Moreover, the T26 position no longer appears to be under selective constraint in SpmX. The
 176 conservation of the GH motif coupled with the apparent inactivation of the catalytic triad across
 177 all SpmX genes suggests that the catalytic cleft has been remodeled structurally and that the
 178 muramidase domain may therefore not retain the same level of activity or function as phage
 179 GH24v lysozymes.

181 **The SpmX muramidase domain has a wider, more dynamic catalytic cleft than related**
 182 **phage lysins.** Obtaining the structure of the SpmX muramidase domain (residues 1-150) from
 183 *Asticcacaulis excentricus* (SpmX-Mur-*Ae*) (**Table S2**) allowed us to directly visualize the effect
 184 of the D20L and T26X mutations on the catalytic cleft. Overall, SpmX-Mur-*Ae* exhibits the

185 characteristic T4 lysozyme structure: the predicted catalytic glutamate occurs at the C-terminal
 186 end of the first alpha-helix, within the catalytic cleft formed between the N- and C-terminal lobes
 187 (**Figure 3A**). P22 lysozyme (the model for molecular replacement) and the active conformation
 188 of the distantly related SAR endolysin protein R21 (PDB 3HDE) from bacteriophage P21
 189 (**Figure S2**) are overlaid in the structural alignment in **Figure 3A** to emphasize the manner in
 190 which the SpmX muramidase domain deviates from these phage lysozymes: besides the
 191 extended beta-hairpin in the C-terminal lobe, the canonical GH beta-hairpin in the N-terminal
 192 lobe of SpmX-Mur-*Ae* splays away from the catalytic cleft relative to those of the phage
 193 lysozymes. This GH beta-hairpin region exhibited the most conformational differences among
 194 the three molecules of SpmX-Mur-*Ae* in the asymmetric unit. The overlay of the three SpmX-
 195 Mur-*Ae* chains in **Figure 3B** illustrates how the orientation of the GH beta-hairpin is tilted by
 196 about 16° between chains A and B, suggesting a heightened flexibility in this region compared to
 197 other T4L-like lysozymes, which may reduce the ability of the enzyme to coordinate
 198 peptidoglycan hydrolysis in the catalytic cleft.

199 GH motif sequence alignments (**Figure 2B**) show that SpmX muramidase domains have
 200 lost a highly conserved tyrosine residue at position 18. Although T4L enzymatic activity is not
 201 sensitive to mutation at this position [27], it is invariant across all the phage lysozyme classes we
 202 analyzed. Visualization of Y18 in the P22 lysozyme structure (**Figure 3C**) shows that it interacts
 203 with R14 at the base of the beta-hairpin, possibly a critical interaction for coordinating the beta-
 204 hairpin with the catalytic glutamate. In SpmX-Mur-*Ae*, Y18S still appears to make hydrogen-
 205 bonding contact with R14; however, most SpmX muramidase domains have non-polar residues
 206 at position 18 (**Figure 2B(iv)**), which may reduce coordination. It has been previously shown
 207 that the Y18 position is a hot-spot for compensatory mutations that restore activity to inactive
 208 catalytic mutants [31], and it is intriguing to imagine that mutations at this position in SpmX
 209 muramidase are associated with the ability of its remodeled, more flexible catalytic cleft to still
 210 bind and/or cleave peptidoglycan.

211 **Figure 3** shows the catalytic clefts of both P22 lysozyme (**D**) and SpmX-Mur-*Ae* (**E**). In
 212 P22 lysozyme, the E11-carbonyl, D20-carboxyl, and T26-hydroxyl groups point into the aqueous
 213 catalytic cleft. In SpmX-Mur-*Ae*, the cleft is slightly reorganized, with the T26M S-methyl
 214 thioether still within 20 Å of E11 and potentially capable of interacting with peptidoglycan. In
 215 about two thirds of the SpmX genes, position 26 is either a valine or an isoleucine, which do not
 216 have any polar moieties to contribute to the cleft (**Figure 2B(iv)**). With this structural data, we
 217 can infer that the SpmX muramidase domain has a remodeled catalytic cleft with a correctly
 218 positioned catalytic glutamate. However, the increased flexibility between the GH motif and the
 219 glutamate, as well as the loss of key coordinating residues might reduce, if not eliminate, SpmX
 220 hydrolytic activity, and would explain why previous groups could not detect hydrolytic activity
 221 from purified SpmX muramidase [18].

222
 223 **SpmX retains reduced hydrolytic activity on peptidoglycan.** Given SpmX's reported
 224 inactivity [18] and the structural data suggesting the catalytic cleft is capable of interacting with
 225 peptidoglycan, we hypothesized that the domain retains ancestral function in binding
 226 peptidoglycan. To test this, various constructs from *C. crescentus*, *A. excentricus*, and *A.*
 227 *biprosthecum* were purified and incubated with sacculi from all three species. Both muramidase
 228 and entire soluble domains including the intermediate domain bound sacculi from all three
 229 species (**Figure S3**). Since the purified protein was capable of binding its putative substrate, we
 230 also tested its ability to hydrolyze peptidoglycan. We used remazol brilliant blue (RBB) assays to

231 compare the activity of SpmX muramidase from *C. crescentus* (SpmX-Mur-*Cc*) to P22 lysozyme
232 (P22Lyso) and its D20L mutant (P22Lyso-D20L) (**Figure 4A**), and found that both SpmX-Mur-
233 *Cc* and P22Lyso-D20L exhibit similarly attenuated hydrolytic activity in comparison to
234 P22Lyso. Both reached maximal levels of RBB release near enzyme concentrations of 15 μ M
235 while P22Lyso reached the same levels near 5 μ M. Mutants in which the catalytic glutamate was
236 replaced with alanine (SpmX-Mur-*Cc*-E11A and P22Lyso-E11A) did not exhibit activity
237 (**Figure S4A**). These data indicate that the “inactivating” substitution D20L attenuates enzymatic
238 activity whereas mutating the catalytic glutamate abolishes it altogether.

239 Because the D20L mutation reduced P22Lyso’s activity close to that of SpmX
240 muramidase, it was possible that this mutation was responsible for SpmX’s attenuated activity.
241 However, restoring the ancestral D20 (SpmX-Mur-*Cc*-L20D) did not increase SpmX activity *in*
242 *vitro* (**Figure S4B**). We suspect that the additional accumulation of mutations in SpmX
243 muramidase, such as the drift observed at Y18 and T26 in the cleft, has made it impossible to
244 restore ancestral phage lysozyme activity with a single mutation. Because the D20L mutation is
245 ancestral in the SpmX phylogeny (**Figure 1B**) and capable of attenuating P22 lysozyme activity
246 to SpmX-like levels, we infer that this mutation likely occurred first. The increased flexibility of
247 the GH motif observed in the SpmX-Mur-*Ae* structure is therefore the consequence of many
248 mutations that accumulated either neutrally after the D20L substitution attenuated the activity, or
249 selectively to shape the new function of the domain as part of SpmX.

250 The enzymatic activity of the P22Lyso-D20L was puzzling in light of early work that
251 reported that D20 mutations inhibited T4 lysozyme in phage plaque assays [27]. One possible
252 explanation is that the D20L mutation reduces lysozyme activity to the point that it is not suitable
253 for cell lysis at *in vivo* expression levels, and that T4 lysozyme with the mutation was unable to
254 complete infection and form plaques. To explore this possibility, we designed an experimental
255 system to test the activity of P22Lyso and SpmX-Mur-*Cc* mutants in the *E. coli* periplasm using
256 fusions to the N-terminal PelB leader sequence (pET22b). Lemo21(DE3) cells expressing
257 P22Lyso lysed without induction (**Figure 4B**), indicating that marginal P22Lyso levels can drive
258 cell lysis. In contrast, cells expressing P22Lyso-D20L lysed only after induction (**Figure 4C**),
259 confirming that much higher enzyme concentrations were needed. Thus the D20L mutation may
260 represent a critical detoxification step that reduced the ability of the domain to lyse the cell and
261 made it available for co-option.

262 Although purified P22Lyso-D20L and SpmX-Mur-*Cc* had similar activation curves *in*
263 *vitro*, Lemo21(DE3) strains expressing SpmX-Mur-*Cc* never lysed (**Figure 4C**). This was
264 despite equivalent periplasmic expression levels to P22Lyso-D20L (**Figure S4D**). Different
265 growth conditions and media increased the amount of SpmX-Mur-*Cc* in the periplasm but did
266 not affect cell viability (**Figure S4C**). Moreover, SpmX-Mur-*Cc* was active on sacculi isolated
267 from Lemo21(DE3) (**Figure S4E**), eliminating the possibility that it could not cleave *E. coli*
268 peptidoglycan. It is possible that SpmX-Mur-*Cc* cannot fold correctly in the *E. coli* periplasm, or
269 that its activity is further attenuated in the periplasmic environment. However, the periplasmic
270 expression tests in *E. coli* confirm that the D20L mutation attenuates P22Lyso hydrolytic activity
271 and thereby increases the amount of protein required to induce lysis. This tuning of enzymatic
272 activity might have served as a critical detoxifying step in the co-option of the muramidase
273 domain from phage. Because SpmX has retained the ancestral catalytic glutamate and its
274 modified catalytic cleft is capable of hydrolytic activity, we conclude that this attenuated activity
275 is under purifying selection in SpmX and must be important for SpmX function.
276

277 **Inactivating the muramidase domain interferes with SpmX localization *in vivo*.** To
 278 determine the role of the preserved, albeit attenuated, activity of the muramidase domain in
 279 SpmX function, we inactivated it by mutating the conserved catalytic glutamate to alanine
 280 (E11A, E19A in SpmX numbering) at the chromosomal locus in various species and observed
 281 the effects *in vivo* (**Figure 5**). We determined the effects of the E11A mutation on cellular
 282 morphology, as the *C. crescentus*, *A. excentricus*, and *A. biprosthhecum* Δ *spmX* strains all have
 283 morphological phenotypes (**Figure 5ABCii**): In *C. crescentus*, Δ *spmX* cells have a characteristic
 284 elongated morphology resulting from failed division cycles and often grow stalks prematurely
 285 from daughter cells that fail to divide completely (**Figure 5Aii**) [15]. In *Asticcacaulis*, Δ *spmX*
 286 cells lack stalks without other apparent developmental phenotypes (**Figure 5BCii**) [17]. If
 287 enzymatic activity is critical for overall SpmX function, we expected that eliminating catalytic
 288 activity with the E11A mutation would phenocopy Δ *spmX*. However, we observed intermediate
 289 phenotypes for this mutation. In *C. crescentus*, the E11A mutant population contained both WT-
 290 like cells and cells exhibiting the division defect, but with less severity than in Δ *spmX* (**Figure**
 291 **5Aiii**). In both *Asticcacaulis* species, the E11A mutants still grew stalks (**Figure 5BCiii**).
 292 Nevertheless, the *A. biprosthhecum* E11A mutant exhibited a significant loss of bilateral stalks
 293 (3.5 fold reduction) and an increase in the frequency of cells with a single stalk (**Figure S5D**).
 294 These results suggest that eliminating catalytic activity does not fully inhibit SpmX function.

295 WT and mutant SpmX GFP fusions allowed us to monitor changes in SpmX cellular
 296 localization. As shown previously [15,17], WT SpmX localized at the future position of the stalk,
 297 at the pole as in *C. crescentus*, or at sub-polar or bilateral positions in *Asticcacaulis*, and was
 298 retained at this position during stalk elongation (**Figure 5ABCiii**). Both *C. crescentus* and *A.*
 299 *biprosthhecum* *spmX* E11A mutants exhibited an increase in delocalized fluorescence throughout
 300 the cell body compared to WT (**Figure 5ABiv**). Quantification of the fluorescence data indicated
 301 that while the overall mean cell fluorescence was the same as WT, the SpmX foci were
 302 significantly less intense in the mutants (**Figure S5AB**). We also observed a 3X increase in the
 303 stalk fluorescence in *A. biprosthhecum* expressing SpmX E11A compared to WT (**Figure S5B**).
 304 Although no difference in focal fluorescence intensity was observed in *A. excentricus* *spmX*
 305 E11A mutant cells, more cells had a second SpmX focus at stalk tips than WT cells (**Figure 5iv,**
 306 **S5C**), indicating altered localization. Western blots of cells expressing WT SpmX-eGFP and
 307 SpmX mutants confirmed that the delocalized fluorescence was not due to clipping of the GFP
 308 tag, but to delocalized SpmX protein (**Figure S5E**). Together these data show that the E11A
 309 mutation disrupts SpmX localization in all three species and may underlie the morphological
 310 defects observed in *C. crescentus* and *A. biprosthhecum*.

311 Because the E11A intermediate phenotype suggested that the mutation might be
 312 disrupting SpmX localization by interfering with peptidoglycan interactions, we also mutated a
 313 position associated with peptidoglycan binding, but not catalysis, in T4 lysozyme. N/Q105 has
 314 been shown to coordinate peptidoglycan in the active cleft [32] and the mutation Q105R
 315 abolished activity in T4 phage plaque assays [27]. The mutation N105R (N91R in SpmX
 316 numbering) in *C. crescentus* and *A. biprosthhecum* resulted in similar delocalization and
 317 intermediate morphological phenotypes as E11A (**Figure 5BCiiv**). We also investigated the
 318 effects of restoring the phage active site D20 (L28D in SpmX numbering) to the catalytic cleft.
 319 However, this had no evident effect on SpmX localization or cell morphology (**Figure 6i**),
 320 suggesting that the D20L substitution in SpmX, while ancestral, is not strictly necessary for
 321 SpmX function. This finding is in line with the observation that SpmX-Mur-*Cc*-L20D activity
 322 was not significantly different from WT in our *in vitro* RBB assays (**Figure S4B**). Therefore, the

323 D20L substitution was likely a key first step in SpmX detoxification but no longer appears to be
324 under fitness constraints.

325 Overall, these data show that inactivating enzymatic activity or reducing the
326 peptidoglycan-binding capability of the muramidase domain affects SpmX localization and
327 function. Although it is not clear whether disrupting SpmX localization with the E11A mutation
328 stems from eliminating SpmX's hydrolytic activity or decreasing SpmX's binding affinity for
329 peptidoglycan, the similar phenotype from mutating a predicted peptidoglycan-interacting
330 residue (N105R) underscores the importance of SpmX-peptidoglycan interactions. That the
331 catalytic mutant has an intermediate morphological phenotype in *C. crescentus* and one
332 *Asticcacaulis* species indicates that the muramidase domain may coordinate SpmX functions
333 similarly in the two genera and that this function likely relies on its interactions with
334 peptidoglycan.

335
336 **Replacing the muramidase domain, or removing it, depletes native SpmX protein levels *in***
337 ***vivo*.** Because SpmX localization depended on the ability of the muramidase domain to interact
338 with peptidoglycan, we were interested in whether swapping alternative muramidase domains
339 into SpmX would support WT function. We first made chimeras wherein P22 lysozyme replaced
340 the domain with the hypothesis that (1) P22 lysozyme would be too active and therefore toxic to
341 the cells and that (2) P22 lysozyme E11A might be able to support some level of SpmX
342 localization. While SpmX and the SpmX-E11A mutant exhibited the previously determined
343 morphological and delocalization phenotypes (**Figure 6Aiii-iv**), chimeras with P22 lysozyme
344 were surprisingly viable but phenocopied the parent Δ *spmX* strain and lacked fluorescence. We
345 were unable to detect any GFP-fusion products in this chimera by Western blot (**Figure 6B**), but
346 confirmed by sequencing that P22Lyso-SpmX had been correctly inserted at the *spmX* locus,
347 suggesting that the chimeras were likely expressed but quickly degraded in *C. crescentus*.
348 Therefore the phenotype of this chimera is due to the loss of SpmX and not the addition of the
349 P22 lysozyme domain. Inactivating P22 lysozyme (E11A) did not change the outcome,
350 suggesting that the toxicity of the phage muramidase was not driving SpmX degradation.

351 To determine whether the loss of SpmX protein levels was particular to using P22
352 lysozyme, we verified the phenotype when SpmX lacked the muramidase domain entirely.
353 Deletion of the muramidase domain from the *spmX* locus in all three species also resulted in
354 strains with the Δ *spmX* phenotype that failed to produce detectable amounts of Δ mur-SpmX-
355 sfGFP by Western blot (**Figure S5E**). These results suggest that the SpmX muramidase domain
356 is necessary to produce and/or maintain WT levels of SpmX in all three species, and that P22
357 lysozyme, despite high sequence similarity (51%) and structural homology (RMSD 1.7 Å), is not
358 sufficient to replace it. P22Lyso and SpmX-Mur-*Cc* are nonetheless fairly distantly related, so
359 we tested the ability of other SpmX muramidase domains to replace that of *C. crescentus*.
360 Previously, *C. crescentus* and *Asticcacaulis* muramidase domains were shown to be
361 interchangeable [17], so we extended the sequence distance to SpmX muramidases from the next
362 closest relative *Brevundimonas subvibrioides*, which has D20R in the catalytic cleft, and the
363 most distant relative *Parvularcula bermudensis*, which shares the D20L mutation. We found that
364 the muramidase domain from *B. subvibrioides* supported the WT phenotype in *C. crescentus*
365 (**Figure 6v**), but that the SpmX muramidase domain from *P. bermudensis* did not. We were
366 surprised to see no evidence of delocalization in the *B. subvibrioides* SpmX chimera because the
367 L20R point mutant of SpmX in *C. crescentus* showed some delocalization (**Figure 6vi**). This
368 result suggests that the L20R mutation in the brevundimonads must coexist with other

369 compensatory mutations. The SpmX muramidase domain from *P. bermudensis*, like P22
370 lysozyme, must be too distant from *C. crescentus* to support WT expression levels. In
371 combination with data from the P22Lyso chimeras, these data indicate that a T4L GH fold alone
372 is not sufficient for SpmX function, and that the SpmX muramidase domain must contain other
373 mutations necessary for stable protein levels in Caulobacterales. It could suggest that this domain
374 has additional constraints on it unrelated to potential peptidoglycan interactions, such as binding
375 interfaces specific to its function as a recruiting factor and protein scaffold.

376

377 Discussion

378

379 Bacteriophages shape bacterial evolution in various ways: they increase bacterial diversity by
380 selectively preying on species [2,33], drive horizontal gene transfer [8,34], and serve as
381 reservoirs of raw material for genetic innovation [35,36]. Phages are heralded as a major source
382 of genetic material for novel gene emergence in bacteria [2,35,36], but, as we discuss later in this
383 section, very few examples of novel gene emergence from prophage exist in the literature. We
384 have investigated the origin and function of a taxonomically restricted gene from
385 Caulobacterales, *spmX*, and determined that its occurrence is the result of the fusion and
386 domestication of a phage peptidoglycan hydrolase gene. Although SpmX functions as a scaffold
387 in developmental regulation and morphology, its muramidase domain retains high sequence
388 similarity to phage lysozymes, which are toxic to bacteria. The active cleft contains mutations
389 that have attenuated the toxic activity of the domain, presumably making it available for genetic
390 innovation and bacterial use. We show here that the domain remains enzymatically active on
391 peptidoglycan and that eliminating this activity alters the function of the full-length protein *in*
392 *vivo*. Thus, the SpmX gene represents a core gene innovation specific to the Caulobacterales
393 order that originally arose from a prophage gene with antibacterial activity.

394 Previously, it was suggested that the SpmX muramidase domain functions only in
395 protein-protein and self-oligomerizing interactions in SpmX's role as a developmental regulator
396 and scaffold in *C. crescentus* [18]. This conclusion was based on the lack of detectable activity
397 from the purified domain and the inability of the catalytic E11R (E19R in SpmX numbering)
398 mutant to self-oligomerize. It is highly likely that the E11R mutation greatly destabilizes the
399 muramidase domain structure. We found that even the E11A mutant eluted in multiple fractions
400 during purification, indicating decreased conformational stability. Moreover, the E11R protein
401 product was no longer detectable in the cells expressing the gene [18]. Thus, the effect of the
402 E11R mutation is similar to using a distantly related muramidase domain (like P22Lyso) or
403 deleting portions of the muramidase domain entirely [15]. These data indicate that the
404 muramidase domain plays an unanticipated role in maintaining stable SpmX protein levels across
405 all tested species: without an appropriate muramidase domain, SpmX is misfolded,
406 misprocessed, and/or quickly degraded.

407 Inactivating the SpmX muramidase domain resulted in developmental defects in *C.*
408 *crescentus* and significant decrease in bilateral stalks in *A. biprosthecum*. Curiously, inactivating
409 the enzymatic domain did not yield a null phenotype or complete delocalization. It is possible
410 that enough peptidoglycan-interactions are maintained in the mutants for the domain to function
411 as a peptidoglycan-binding domain. It is also possible that SpmX recruits proteins with
412 redundant enzymatic activity that cannot be recruited in the Δ *spmX* mutant, as it is already
413 known that SpmX interacts with targeting factors via its C-terminal domains in *Asticcacaulis*
414 [17] and possibly via its transmembrane segments with DivJ [15]. Finally, it is hard to

415 distinguish whether there is a direct relationship between catalytic activity and peptidoglycan
416 binding, or if cleaving peptidoglycan could indirectly localize SpmX. The multiple domains and
417 pleiotropic effects of SpmX make it difficult to assess the effects of an individual domain on its
418 *in vivo* function. However, our data support a model in which the muramidase domain of SpmX
419 is still active, and this activity is used to localize SpmX. We conclude that the muramidase
420 domain functions in localizing SpmX via its interactions with peptidoglycan rather than self-
421 oligomerization as previously hypothesized. This proper localization is necessary for its roles in
422 development and morphology.

423 SpmX emerges in the genomic record at the root of Caulobacterales with the attenuating
424 D20L mutation (**Figure 1B**). The D20L mutation is therefore ancestral and potentially the initial
425 step in the co-option of the domain. D20L conservation throughout most of Caulobacterales
426 suggests evolutionary constraint on this position despite no observable phenotype from the
427 SpmX-Mur-Cc L20D reversion mutation *in vivo* or *in vitro*. After the D20L substitution
428 detoxified the muramidase domain, the domain likely accumulated both neutral and occasional
429 adaptive mutations in the context of its new function. The active cleft contains several
430 modifications, including the loss of selection on the third catalytic triad position, T26, and the
431 invariant residue Y18. This pair is interesting in that Y18 was identified as a hotspot for
432 spontaneous second site revertants of T26 mutants in T4 lysozyme [31]. It is possible that the
433 changes we see at these two positions are compensatory mutations retaining attenuated activity,
434 although there is no clear history of covariation. Accumulation of these types of mutations likely
435 underlies the inability to restore phage lysozyme-like activity by reversing the D20L substitution.
436 The ancestral D20L mutation has diverged in two groups: *Oceanicaulis* and *Maricaulis*
437 (D20R/G), and *Brevundimonas* (D20R) (**Figure 1B, S1**). Interestingly, D20R/G is covariant with
438 residue N105S/D (**Figure S1**), a peptidoglycan-interacting residue in T4L [32]. The covariance
439 of peptidoglycan-interacting residues in these diverging genera further underscores the
440 importance of this domain in peptidoglycan interactions, rather than just protein-protein
441 interactions.

442 *spmX* arose recently enough to see the hallmarks of novel gene emergence and adaptation
443 in a constrained bacterial clade. The gene either arose from a fusion event in the bacterial
444 genome, or the original phage gene contained the transmembrane segments. Detoxification of the
445 muramidase appears concomitant with the origin of the full SpmX gene comprising three fused
446 domains. Maintenance of the muramidase domain since the emergence of SpmX and its activity
447 in current living Caulobacterales members suggest that its attenuated activity was selected for in
448 the ancestral protein and still involved in its modern functions. In contrast, SpmX's downstream
449 intermediate domain is highly variable throughout Caulobacterales (**Figure 1A**). This domain
450 appears to experience comparatively minimal sequence constraint and has undergone multiple
451 independent events of elaboration and reduction in this clade. This region of charged residues
452 and prolines drives SpmX self-oligomerization *in vitro* [18], and may also facilitate other protein
453 interactions. For example, the intermediate domain appears to be responsible for targeting SpmX
454 to sub-polar and bilateral positions in *Asticcacaulis* [17].

455 In several reported cases bacteria have domesticated phage genes for genetic
456 manipulation and transfer, bacterial warfare, virulence, and secretion. However, these events are
457 distinct from that which created the novel bacterial gene *spmX*. Phage genes for DNA replication
458 and recombination have replaced bacterial functional homologues within bacterial genomes
459 several times [37–40], however these genes retain their original function and carry out the same
460 tasks. Gene transfer agents (GTAs) pose an interesting case where virion proteins from cryptic

461 prophage package random DNA from the bacterial genome to presumably share with other
462 bacteria [41]. Although a specific GTA has been stably maintained across several
463 alphaproteobacterial orders, this domesticated island of phage genes still shuttles DNA around,
464 as it once did in ancestral infectious cycles [42,43]. Phage tails have been weaponized many
465 times, resulting in type VI secretion systems [44,45], tailocins and phage tail-like bacteriocins
466 [12–14], phage tail-like systems with insecticidal properties [11,46,47], and phage tail-like arrays
467 [48]. All of these represent a “guns for hire” acquisition scheme in which phage genes are co-
468 opted for their ancestral toxicity and function [2]. Many of these genes reside in genomic islands
469 and confer environmental, niche-specific advantages that directly exploit their ancestral activity
470 for the benefit of the host. Similarly, in two other known cases of phage lysozyme domestication
471 in bacteria, muramidase domains have been fused to colicins [49] or are predicted to be secreted
472 with type III secretion systems [50], presumably for use in bacterial warfare or infection. In one
473 strange case, a phage lysozyme gene has been co-opted in bivalve genomes, which apparently
474 still use the gene for its antibacterial properties [51].

475 The domestication of the muramidase domain in SpmX is distinct from the above cases
476 of “guns for hire” because the phage gene has been incorporated into a novel bacterial gene with
477 new function in basic cellular processes in a large bacterial order. The SpmX muramidase
478 domain, although active, no longer lyses bacterial cells; instead it plays a role in localizing
479 SpmX for its function in developmental regulation and morphogenesis. The co-option of phage
480 genes for core cellular function is likely a common event in nature, but identifying such genes
481 may require a careful search. Based on our findings, we suggest a future strategy for their
482 detection: searching for phage gene homologues with long histories of vertical inheritance and
483 signs of innovation in bacterial genomes.

484 **Acknowledgements**

486 We thank members of the Brun, Vernet, and Dessen laboratories for support, advice and
487 encouragement. Many thanks to Breah LaSarre, Farrah Bashey-Visser, Jay Lennon, Daniel
488 Schwartz, and Ernesto Vargas for critical manuscript reading and editing. Enthusiastic thanks for
489 critical preprint review by the journal clubs of the (Pamela) Brown Lab (University of Missouri)
490 and the Süel Lab (UCSD). We thank David Flot (ESRF, beamline ID30a1) for support in data
491 collection. The NIH supported this work with grants 2R01GM051986 and R35GM122556 (to
492 Y.V.B.), and NRSA F32GM112362 (to A.M.R.). A Fulbright US Research Scholar Award
493 supported the work of Y.V.B. at the Institut de Biologie Structurale in Grenoble. Y.V.B. is
494 supported by a Canada 150 Research Chair in Bacterial Cell Biology. This work used the
495 platforms of the Grenoble Instruct-ERIC Center (ISBG : UMS 3518 CNRS-CEA-UGA-EMBL)
496 with support from FRISBI (ANR-10-INSB-05-02) and GRAL (ANR-10-LABX-49-01) within
497 the Grenoble Partnership for Structural Biology (PSB).

498 **Author Contributions**

500 Conceptualization, A.M.R. and Y.V.B.; Methodology, A.M.R., D.T.K., C.M., and Y.V.B.;
501 Investigation, A.M.R. with the following exceptions - D.T.K. performed the sequence
502 conservation analysis (Figure 1A) and the phylogenetic analysis (Figure 1B), Y.V.B. grew
503 crystals, and C.M. collected X-ray diffraction data and solved the crystal structure; Resources,
504 C.M. and Y.V.B.; Writing – Original Draft, A.M.R.; Writing – Review and Editing, A.M.R.,
505 D.T.K., C.M., and Y.V.B.; Visualization, A.M.R.; Supervision, C.M. and Y.V.B.; Funding
506 Acquisition, A.M.R., C.M., and Y.V.B.

507
 508
 509
 510
 511
 512
 513
 514
 515
 516
 517
 518
 519
 520
 521
 522
 523
 524
 525
 526
 527
 528
 529
 530
 531
 532
 533
 534
 535
 536
 537
 538
 539
 540
 541
 542
 543
 544
 545
 546
 547
 548
 549
 550
 551
 552

Declaration of Interests

The authors declare no competing interests.

Main Figure Titles and Legends

Figure 1. The SpmX is vertically inherited in Caulobacterales. (A) Schematic of SpmX architecture, including the conserved muramidase domain (see **Figure S1** for alignments), the variable intermediate domain, and two C-terminal transmembrane (TM) segments. Bar indicates amino acid sequence conservation among *spmX* alleles (see **Table S1** for a list of *spmX* genes used in this study). (B) Phylogenetic trees of representative species from Caulobacterales and other Alphaproteobacteria for concatenated housekeeping gene alignments (left) and for SpmX (right), with branch colors indicating the amino acid identity at position 20 of SpmX (D20L in yellow, D20R in red, and D20G in green). See **Table S6** for genome IDs. The concatenated housekeeping tree is fully supported with posterior probability of 1.0 for all clades. Asterisks indicate clades in the SpmX tree with posterior probabilities > 0.95. See **Figure S2** for the relationship of the SpmX muramidase domain within the lysozyme superfamily.

Figure 2. The SpmX muramidase domain retains the canonical GH motif but contains inactivating mutations in the catalytic cleft. (A) P22 lysozyme (PDB 2ANX) as a model lysozyme colored with rainbow gradient from blue N-terminus to red C-terminus. The catalytic glutamate appears in fuchsia and the GH beta-hairpin in light blue. (B) HMM logos of GH lysozymes made using WebLogo 3 [52]. Logos were constructed from protein sequences of (i) T4 lysozyme-like genes (n = 94), (ii) representative autolysins/endolysins from the Conserved Domain Database including P22 lysozyme (n = 20) but excluding SpmX genes, (iii) closest BLAST hits from non-SpmX muramidases (n = 60), and (iv) SpmX muramidases (n = 66), and organized in a cladogram to resemble the sequence cluster tree diagram in **Figure S2**. Amino acids are color-coded according to chemical properties, with uncharged polar residues in green, neutral residues in purple, basic residues in blue, acidic residues in red, and hydrophobic residues in black. The height of each letter is proportional to the relative frequency of a given identity and the height of the stack indicates the sequence conservation at that position. T4L numbering is used for ease of comparison. Asterisks mark positions critical for enzymatic activity and open circles mark positions associated with GH motif stability [26,27]. Refer to **Figure S1** for alignments of SpmX muramidases, which are listed in **Table S1**. See also **Table S5** for non-SpmX GH24 gene IDs.

Figure 3. The structure of SpmX muramidase domain has a wider, more dynamic catalytic cleft than related phage lysins. (A) Structural alignment of P22 lysozyme (PDB 2ANX, the model used for molecular replacement) in purple, R21 endolysin from P21 (PDB 2HDE, a distantly related GH24 T4L lysozyme) in navy blue, and SpmX-Mur-*Ae* in gold (PDB 6H9D). The catalytic glutamate is shown in red. Root mean square deviation (rmsd) 1.7 Å and 40% identity over 141 aligned Cα atoms, Dali Z-score 21.5 between P22 lysozyme and SpmX-Mur-*Ae*. See **Table S2** for data collection and refinement statistics. (B) Structural alignment of the three SpmX-Mur-*Ae* molecules, chains A (green), B (light blue), and C (dark blue), from the asymmetric unit. The surface of chain B is shown in partially transparent light blue. The double-headed arrow indicates the tilt of about 16° between the GH beta-hairpins of chains B and A. (C)

553 Overlays of ribbon diagrams and surfaces of P22 lysozyme (2ANX, left) and SpmX-Mur-*Ae*
 554 (6H9D, right) illustrating the conformation of the critical residues E11 (red), D20 (dark blue),
 555 R14 (yellow), and Y18 (orange). T4L numbering is used for ease of comparison. These
 556 structures have been rotated 180° around the y-axis from their representation in (A, B, D, E). **(D)**
 557 Surface representation of P22 lysozyme (2ANX) with inset showing ribbon diagram and
 558 conformation of catalytic cleft with the canonical E11/D20/T26 catalytic triad. **(E)** Surface
 559 representation of SpmX-Mur-*Ae* (6H9D) with inset showing ribbon diagram and conformation of
 560 remodeled catalytic cleft with E11/D20L/T26M.
 561

562 **Figure 4. The D20L mutation attenuates P22 hydrolytic activity.** **(A)** Remazol brilliant blue
 563 assays on *C. crescentus* sacculi using purified P22 lysozyme, P22 lysozyme D20L mutant, and
 564 *C. crescentus* SpmX muramidase. Active enzymes release peptidoglycan monomers covalently-
 565 bound to RBB into the supernatant that are detected by absorbance at 595 nm. Error bars are ±
 566 standard deviation for each normalized absorbance (n = 3). Lines are drawn to help guide the eye
 567 toward basic trends. Data points are from various days and sacculi preparations, but with internal
 568 normalization to Hen Egg White Lysozyme (HEWL). See **Figure S3** for peptidoglycan binding
 569 activity and **Figure S4AB** for SpmX mutant activity in RBB assays. **(B and C)** Growth curves of
 570 Lemo21(DE3) *E. coli* expressing P22 lysozyme (blue), P22 lysozyme D20L mutant (green), and
 571 *C. crescentus* SpmX muramidase (red). Proteins were expressed from pET22b with a N-terminal
 572 PelB signal sequence. In **(B)**, strains were grown in 5 mM rhamnose without IPTG for maximal
 573 repression of basal expression from the plasmids. In **(C)**, strains were grown without rhamnose
 574 and induced with 400 μM IPTG at the indicated time. See **Figure S4CDE** for enzymatic activity
 575 and periplasmic expression of SpmX-Mur and various mutants. **(D)** Phase/fluorescent overlays
 576 show live/dead staining of Lemo21(DE3) cells expressing P22Lyso-D20L and SpmX-Mur-*Cc*
 577 after four hours of induction. Green, membrane permeable SYTO 9 stains DNA in live cells and
 578 red, membrane impermeable propidium iodide nucleic acid dyes labels released nucleoids and
 579 DNA from lysed bacteria. The rounding of the *E. coli* in (i) is characteristic of spheroplast
 580 formation and lysis by hydrolytic activity on the cell wall. Scale bars are 5 μm.
 581

582 **Figure 5. Inactivating the muramidase domain partially delocalizes SpmX in vivo.**
 583 Phase and fluorescent images of **(A)** *C. crescentus*, **(B)** *A. biprosthecum*, and **(C)** *A. excentricus*.
 584 In the top panel, phase images with derived schematics emphasizing stalks and morphologies are
 585 shown for **(i)** WT and **(ii)** Δ *spmX* cells. In **Aii**, *C. crescentus* cells exhibiting characteristic
 586 Δ *spmX* divisional defects are marked with asterisks and a cell growing stalks from both poles has
 587 its stalks marked with red arrowheads. Phase and fluorescent images of cells expressing **(iii)**
 588 SpmX-eGFP, **(iv)** SpmX-E11A-eGFP, or **(v)** SpmX-N105R-eGFP from the native chromosomal
 589 locus are shown in the lower panels. In **Aiv** and **Av**, cells with divisional defects are marked with
 590 white asterisks. In **Biii** and **Biv**, cells with one lateral or subpolar stalk are marked with white
 591 arrowheads. In **Civ**, cells with foci at the tips of stalks are marked with white arrowheads. All
 592 scale bars are 5 μm. See **Figure S5** for quantification of fluorescence and morphology data.
 593

594 **Figure 6. Removing or replacing the muramidase domain depletes native SpmX protein**
 595 **levels in vivo.** **(A)** Phase and fluorescent images of strains in which the native *spmX* allele was
 596 replaced with the following gene fusions in the Δ *spmX* parent strain **(ii)**: **(i)** *spmX-L20D-sfGFP*
 597 **(iii)** WT *spmX-sfGFP*, **(iv)** *spmX-E11A-sfGFP*, **(v)** *MurBs- Δ mur-SpmX-sfGFP* where *MurBs* is
 598 the muramidase domain from *Brevundimonas subvibrioides* SpmX, and **(vi)** *spmX-L20R-sfGFP*.

599 All scale bars are 5 μm . **(B)** Western blot comparing the ΔspmX parent strain to SpmX mutants
600 and chimeras inserted at the *spmX* locus. In all cases, the primary antibody is directed against the
601 C-terminal GFP fusion.

602

603 **STAR Methods**

604

605 **Contact for Reagent and Resource Sharing**

606 Further information and requests for resources and reagents should be directed to and will be
607 fulfilled by the Lead Contact, Yves Brun (ybrun@indiana.edu).

608

609 **Experimental Model and Subject Details**

610 *E. coli* strains were grown in LB as described in the Method Details sections concerning
611 purification and periplasmic expression. All *C. crescentus*, *A. excentricus*, and *A. biprosthicum*
612 strains used in this study were grown in liquid PYE medium. *C. crescentus* (CB15N/NA1000)
613 was grown at 30°C, and *Asticcacaulis excentricus* (CB48/ATCC 15261) and *Asticcacaulis*
614 *biprosthicum* (C19/ ATCC 27554) species at 26°C. Strains were maintained on PYE plates
615 supplemented with antibiotics as necessary (kanamycin 20 $\mu\text{g}/\text{mL}$, gentamycin 5 $\mu\text{g}/\text{mL}$, and
616 spectinomycin 100 $\mu\text{g}/\text{mL}$). For microscopy, *C. crescentus* and *A. excentricus* were inoculated
617 from colonies, grown overnight, then diluted back 1:50 and grown for another 3-4 hours before
618 being imaged in mid- to late-exponential phase. *A. biprosthicum* was inoculated from colonies
619 and grown overnight to reach mid- to late-exponential phase for imaging. A detailed list of
620 strains is included as **Table S4**.

621

622 **Method Details**

623 **Bioinformatics and gene trees.** Sequences of the SpmX genes in **Table S1** and members of the
624 GH24 family were retrieved by BLAST searches on the Integrated Microbial Genomes and
625 Microbiomes (IMG/M) database [53] and the National Center for Biotechnology Information
626 (NCBI) “nr” database. See **Tables S1** and **S5** for lists of gene ID numbers. Multiple alignments
627 were achieved with MUSCLE [54] and manually adjusted and visualized with Jalview [55].
628 Sequence conservation of SpmX residues was determined from the multiple sequence alignment
629 of *spmX* alleles using ConSeq [56]. To improve visualization of conservation patterns, the
630 ConSeq scores were averaged across a 20-residue sliding window. For estimating bacterial
631 species phylogeny, assembled genome data were obtained from the genome database of the
632 National Center for Biotechnology Information [57]. See **Table S6** for lists of genome IDs.
633 Amino acid sequences of 37 conserved housekeeping genes were automatically identified,
634 aligned, and concatenated using Phylosift [58]. All phylogenetic reconstruction was performed
635 using MrBayes v3.2.6 [59] to estimate consensus phylogenies and clade posterior probability
636 support values. Sequence substitution was modeled according to a WAG substitution model with
637 gamma-distributed rate variation between sites. Trees were visualized and formatted using iTol
638 [60]. The sequence cluster tree was built with NCBI’s Conserved Domain Database tool (CDD)
639 [21,22]. This tool uses reverse position-specific BLAST, a method that compares query
640 sequences to databases of position-specific score matrices and obtains *E*-values, such as in PSI-
641 BLAST [21,22]. WebLogo3 was used to plot the amino acid distribution at each position of the
642 GH motif [52]. To create the alignments for logo generation, 94 T4 lysozyme-like sequences, 20
643 endolysin/autolysins from the CDD analysis, 60 SpmX muramidase-like sequences (BLAST

644 hits), and 66 SpmX muramidase sequences were simultaneously aligned to T4 lysozyme. Only
 645 sequences with unambiguous alignment in the GH motif were included in this analysis.

646
 647 **Recombinant DNA methods.** DNA amplification, Gibson cloning, and restriction digests were
 648 performed according to the manufacturer. Restriction enzymes and Gibson cloning mix were
 649 from New England Biolabs. Cloning steps were carried out in *E. coli* (alpha-select competent
 650 cells, Bioline) and plasmids were purified using Zyppy Plasmid Kits (Zymo Research
 651 Corporation). Sequencing was performed by the Indiana Molecular Biology Institute and
 652 Eurofins MWG Operon Technologies with double stranded plasmid or PCR templates, which
 653 were purified with a DNA Clean & Concentrator kits (Zymo Research Corporation).
 654 Chromosomal DNA was purified using the Bactozol Bacterial DNA Isolation Kit (Molecular
 655 Research Center). Plasmids were introduced into all *E. coli* strains using chemical transformation
 656 according to the manufacturer's protocols. Plasmids were introduced into *C. crescentus*, *A.*
 657 *excentricus*, and *A. biprosthicum* by electroporation based on previously published studies [61].
 658 Briefly, for a given electroporation, 1 mL of culture in early stationary phase was pelleted at
 659 4600 *xg* and washed twice with 1 mL of water. The pellet was resuspended in 50 μ L water and
 660 placed in a 2.0 mm gap electroporation cuvette. 0.5-1 μ g of DNA in 1-5 μ L water was added
 661 before pulsing (2.5 kV, 25 μ F, 200 Ω). The cells were resuspended in 500 μ L PYE, allowed to
 662 recover overnight, and plated the next day on selective plates. Allelic exchange in was achieved
 663 with pNPTS138, large genetic insertions with pMCS-2 [62], and eGFP insertional fusions with
 664 pGFPC-1 and pGFPC-2 [62].

665
 666 **Plasmid construction.** *Expression plasmids:* *spmX* gene fragments encoding amino acids 2-150
 667 of SpmX (SpmX-Mur) were amplified from genomic DNA and inserted into linearized
 668 expression vectors using Gibson cloning (NEB) according to manufacturers protocols. P22
 669 lysozyme (P22Lyso) was amplified from a synthetic gene strand (Eurofins) for similar
 670 construction with Gibson cloning. For pTB147SUMO, the vector was linearized with SapI and
 671 XhoI to insert SpmX-Mur-*Ae*. For pET28a, the vector was linearized with NdeI and EcoRI to
 672 insert SpmX-Mur-*Cc*, BamHI and XhoI to insert SpmX-Mur-*Ae*, SacI to insert SpmX-Mur-*Ab*,
 673 and EcoRI to insert P22Lyso. In all pET28a plasmids, the constructs were cloned in frame with
 674 the N-terminal His-tag and a stop codon to eliminate the C-terminal His-tag. For pET22b, the
 675 vector was linearized with EcoRI and the C-terminal His-tag was preserved. Point mutants in
 676 expression vectors were obtained by using standard "quick-change" site-directed mutagenesis
 677 procedures and primers with 3' single stranded overhangs for increased efficiency.

678 *Integrating plasmids for allelic exchange:* For allelic exchange, the desired mutation was
 679 engineered into pNPTS138, bracketed by 1 kb up- and downstream of the corresponding genetic
 680 region. Integrants were isolated by antibiotic selection and secondary recombination events were
 681 selected by sucrose counter-selection using standard procedures. The resulting clones were
 682 confirmed by PCR and sequencing isolated genomic DNA.

683 For genomic deletions of *spmX* in *Asticcacaulis*, pNPTS138 was linearized with EcoRI
 684 and codons on either end of the gene were retained to avoid introducing frame-shifts in the
 685 surrounding area. Therefore the final gene deletion in *A. excentricus* lacks residues 5-808 and in
 686 *A. biprosthicum* lacks residues 5-815. For SpmX Δ mur truncations, residues 2-150 were removed
 687 in all three species. In all cases pNPTS138 was linearized with EcoRI. Point mutations E19A and
 688 N91R were integrated into the Δ *spmX* background for ease of clone isolation and included full-
 689 length SpmX flanked by 1 kb genetic context. pNPTS138 containing mutated SpmX were

690 constructed using Gibson cloning with fragments on either side of the intended mutation and
691 overlapping primers containing the mutation amplified from genomic DNA. In all cases
692 pNPTS138 was linearized with EcoRV, except for SpmXAb-E19A, where pNPTS138 was
693 linearized with EcoRI.

694 *Plasmids for insertional eGFP fusions:* The last 600 bp of *spmX* from *C. crescentus* was
695 amplified from genomic DNA and cloned into pGFPC-2 using Gibson cloning.

696 *Plasmids for integration at the Δ spmX locus:* These constructs were designed to allow
697 insertion of various SpmX mutants fused to C-terminal sfGFP into the Δ spmX locus in *C.*
698 *crescentus*. For SpmX-sfGFP and SpmX-E19A-sfGFP, fragments containing 1 kb of genomic
699 DNA upstream of *spmX* and *spmX* or *spmX-E19A* were amplified from existing pNPTS138
700 constructs and fused to a fragment containing monomeric sfGFP amplified from pSRKKm-Plac-
701 *sfgfp* [63] using Gibson cloning. In the final construct, SpmX and sfGFP are connected with the
702 linker sequence GSAGSAAGSGEF [64]. Chimeras with P22 lysozyme (P22Lyso) and its
703 catalytic mutant were made by Gibson cloning together fragments containing 1kb of upstream
704 genomic DNA, P22Lyso (with no stop codon), SpmX Δ mur (residues 151-431) and sfGFP with
705 the same linker. P22Lyso and P22Lyso-E11A were amplified from pET28a plasmids containing
706 these genes. Chimeras with SpmX muramidase from *Brevundimonas subvibrioides* (residues 1-
707 140) and *Parvularcula bermudensis* (residues 1-168) were similarly made with the muramidase
708 fragments amplified from genomic DNA and synthetic gene strands (Eurofins), respectively.

709
710 **Production of SpmX-Mur-Ae for crystallography.** The muramidase domain of SpmX from *A.*
711 *excentricus* (SpmX-Mur-Ae, residues 2-150) was fused to a hexahistidine tag followed by the
712 SUMO cleavage site of the Ulp1 protease (His-SUMO tag) [65] and overexpressed in *E. coli*
713 BL21 (DE3) RIL cells. Cells were grown at 37 °C in 2 l of Terrific Broth (BD Biosciences)
714 supplemented with ampicillin (100 μ g/mL) until the OD_{600nm} reached 0.8. Production of the
715 recombinant protein was induced by the addition of isopropyl β -D-1-thiogalactopyranoside
716 (IPTG) to 0.5 mM after the culture was cooled to 25°C. Cell growth was continued overnight at
717 25°C, and cells were harvested by centrifugation. Cell pellets were resuspended in 1/20th volume
718 of buffer A (50 mM Tris-HCl (pH 8.0), 500 mM NaCl, 25 mM imidazole, 10% (vol/vol)
719 glycerol) containing the CompleteTM cocktail of protease inhibitors (Roche). Cells were lysed by
720 six passages through a cell disruptor (Constant Systems Limited) at 20 kPsi, and cell debris were
721 pelleted by centrifugation at 40,000 \times g for 30 min at 4 °C. The centrifugation supernatant was
722 loaded on a Ni-NTA agarose resin (Qiagen) equilibrated with buffer A. After extensive washing
723 with buffer A, His-SUMO-SpmX-Mur-Ae was eluted with a linear 0-100% gradient of buffer B
724 (50 mM Tris-HCl (pH 8.0), 300 mM NaCl, 500 mM imidazole, 10% (vol/vol) glycerol) over 10
725 column volumes. Peak fractions were pooled, mixed with a 1:100 dilution of a His-tagged Ulp1
726 (SUMO) protease preparation [66] and dialyzed overnight at 4°C in buffer C (50 mM Tris-HCl
727 (pH 8.0), 300 mM NaCl, 10% (vol/vol) glycerol). Cleavage reactions were passed through Ni-
728 NTA resin to remove free His-SUMO tag and His-Ulp1, and untagged protein was collected in
729 the flow through. Flow-through fractions were concentrated with Amicon Ultra Centrifugal filter
730 units with a molecular weight cutoff of 10 kDa (Millipore) and were injected onto an ENrichTM
731 SEC650 10x300 gel-filtration column (Biorad). SpmX-Mur-Ae was eluted with buffer D (25 mM
732 Tris-HCl (pH 8.0), 150 mM NaCl) and again concentrated with Amicon Ultra Centrifugal filter
733 units. Protein concentration was measured using absorbance at 280 nm.

734

735 **Protein crystallization and structure determination.** High-throughput crystallization trials
736 were performed with a Cartesian PixSys 4200 crystallization robot (Genomic Solutions, U.K.).
737 Hanging drops containing 100 nL of protein (25 or 12.5 mg/mL) and 100 nL of reservoir
738 solution were set up in 96-well Crystal Quick plates (Greiner) and incubated at 20°C. Initial
739 crystal hits were refined manually by setting up hanging drops containing 1 µL of protein (25 or
740 12.5 mg/mL) and 1 µL of reservoir solution in 24-well plates (Molecular Dimensions) incubated
741 at 20°C. Large needle-shaped crystals (dimensions of about 40 x 40 x 400 µm) were finally
742 obtained for SpmX-Mur-Ae in 0.1 M Tris-HCl pH 8.5, 12% PEG 3350, 0.2 M MgCl₂, at 20°C
743 within 24–48 h. SpmX-Mur-Ae crystals were cryoprotected by transfer into 0.1 M Tris-HCl pH
744 8.5, 13% PEG 3350, 0.2 M MgCl₂, 10% glycerol, and then flash-frozen in liquid nitrogen. X-ray
745 diffraction data were collected at the European Synchrotron Radiation Facility (ESRF, Grenoble,
746 France) on the ID30a1 (MASSIF-1) beamline [67,68].

747 Diffraction data were indexed and scaled using the XDS program suite [69]. SpmX-Mur-
748 Ae crystals belong to the trigonal space group P3₂21, with unit cell dimensions of 100.44 x
749 100.44 x 96.62 Å and three molecules per asymmetric unit. Phase determination was carried out
750 by the molecular replacement method with PHASER [70], using as a search model the structure
751 of the phage P22 lysozyme (PDB entry 2ANX) to 1.9 Å resolution (*R*_{cryst} 21.1%, *R*_{free}
752 25.5%,) (**Table S2**). The molecular replacement solution model was rebuilt de novo using
753 PHENIX [71] to prevent bias from the model.

754 The structure of SpmX-Mur-Ae was completed by cycles of manual building with COOT
755 [72] and addition of water molecules with ARP/wARP [73]. Several cycles of manual building
756 and refinement with REFMAC [74], as implemented in the CCP4 program suite, were performed
757 until *R*_{work} and *R*_{free} converged [75]. Stereochemical verification was performed with
758 PROCHECK [76]. The secondary structure assignment was verified with DSSP [77], with all
759 residues within most favorable or allowed regions of the Ramachandran plot. Figures were
760 generated with PyMol (<http://www.pymol.org>). Coordinates of the final refined model were
761 deposited at the Protein Data Bank (PDB, <http://www.rcsb.org>) and were assigned PDB entry
762 code 6H9D. The data collection and refinement statistics are summarized in **Table S2**.
763

764 **Protein production for *in vitro* assays.** Fresh BL21(DE3) competent cells (Novagen) were
765 transformed with pET28a constructs containing various muramidase genes with N-terminal His-
766 tags and grown overnight in LB with 1% glucose and 50 µg/mL kanamycin. Overnight cultures
767 were diluted 100-fold in LB medium with 1% glucose and 50 µg/mL kanamycin. Typically 500
768 mL cultures of cells were grown for 1.5-2 hours to an OD₆₀₀ of 0.6-0.7 and shifted to 20°C.
769 When the OD₆₀₀ reached 0.8–0.9, the cells were induced with 0.5 mM IPTG. After growing for
770 4 h at 20 °C, cells were harvested and resuspended in 30 mL lysis buffer (25 mM HEPES pH
771 7.5, 100 mM NaCl, 20 mM imidazole, 5 mM BME) with a EDTA-free Protease Inhibitor Mini
772 Tablet (Pierce) and phenylmethanesulfonyl fluoride (PMSF, 1 mM). The 30 mL cell mixture was
773 lysed on ice using a sonicating horn and spun down at 10,000g for 20-30 min. The clarified
774 lysate was loaded onto a 5 ml HiTrap Chelating HP cartridge (GE Healthcare) charged with Ni²⁺
775 and pre-equilibrated with lysis buffer. After loading, the column was washed with lysis buffer
776 followed by an elution via a 0-100% linear gradient of buffer B (25 mM HEPES pH 7.5, 100
777 mM NaCl, 500 mM imidazole, 2 mM BME). Muramidase-containing fractions were pooled
778 based on SDS-PAGE analysis and concentrated to 2.5 mL. Imidazole was removed by passing
779 the concentrated fraction over a PD10 desalting column (GE Healthcare) equilibrated with 25
780 mM HEPES pH 7.5, 100 mM NaCl, 2 mM BME.

781
782 **Sacculi preparation, RBB labeling, and calibration.** Sacculi were prepared from all species in
783 the same manner. For a typical 2L prep, cells were grown to an OD of 0.5-1 in their respective
784 medium (see culturing details in Experimental Model and Subject Details) and harvested by
785 centrifugation at 6,000g for 20 minutes. *C. crescentus* cells usually required multiple
786 centrifugation steps to collect all the cells. Cells were resuspended in 25 mL water (or PBS for *E.*
787 *coli*) and added drop-wise into 50 mL of boiling 7.5% SDS under stirring. The mixture was
788 boiled for 30 minutes and then allowed to cool to room temperature. Sacculi were then pelleted
789 by ultracentrifugation at 100,000g for 30 minutes at room temperature. The resulting pellets were
790 resuspended in 100 mL pure water, and washed repeatedly until SDS was no longer detected in
791 the supernatant. The pellet was confirmed to be clear of SDS by mixing 0.2 mL of the
792 supernatant with 1 μ L 0.5% methylene blue, 0.1 mL 0.7M NaPO₄ pH 7.2, and 0.6 mL
793 chloroform and checking to make sure that, after vortexing and allowing to settle, the solution
794 had an upper blue phase and a lower clear phase [78]. At this point, the pellets were resuspended
795 in 10 mL PBS with 20 mM MgSO₄, 250 U/ μ L Pierce Universal Nuclease (Thermo Fisher
796 Scientific), and 10 mg/mL amylase (Sigma). The mixture was incubated at 37°C for 1-4 hours.
797 Afterwards, 10 mg/mL trypsin and 10 mM CaCl₂ was added and the mixture incubated overnight
798 at 37°C. 800 μ L of 15% SDS were then added to the mixture and it was brought to a boil for
799 about 10 minutes and allowed to cool to room temperature. The sample was then pelleted
800 (100,000g, 30 min, room temperature) and resuspended in 4-5 wash steps until SDS was no
801 longer detected. The final pellet was then resuspended in 2 mL water and added to 0.8 mL 0.2M
802 remazol brilliant blue (Sigma), 0.4 mL 5M NaOH, and additional water to 8 mL. The mixture
803 was incubated, shaking, overnight at 37°C. After neutralizing the solution with 0.4 mL 5M HCl,
804 the mixture was then pelleted (21,000g, 20 minutes, room temperature), and resuspended in
805 water until the supernatant became clear.

806 To calibrate the concentration of RBB-labeled sacculi for dye-release assays and
807 peptidoglycan-binding assays, activity curves with Hen Egg White Lysozyme (HEWL, Sigma)
808 were produced using different dilutions of the RBB-labeled sacculi. The RBB-labeled sacculi
809 were used at the dilution that resulted in an A595 of 0.5 when 5 μ L of the RBB-labeled sacculi
810 were incubated with 4 μ M HEWL.

811
812 **Peptidoglycan-binding assays.** 5 μ L of calibrated RBB-labeled sacculi were incubated with 1 μ M
813 of purified protein (protein constructs used are shown in Figure S4) in PBS pH 7.4 to a final
814 volume of 50 μ L for 30 minutes at 37°C and then pelleted (16,000g, 20 minutes). Fractions were
815 separated and the pellet resuspended in 50 μ L PBS. 10 μ L of each fraction was loaded onto Any
816 kD Mini-PROTEAN TGX Precast Protein Gels (BioRad) to visualize whether the protein
817 associated with the insoluble sacculi fraction. BSA (Sigma) was used at 1 μ M as a negative
818 control.

819
820 **Remazol brilliant blue dye-release assays.** Methods were adapted from [79,80]. Assays were
821 carried out in 25- μ L reactions using 25 mM HEPES pH 7.5, 100 mM NaCl and 5 μ L of
822 calibrated RBB-labeled sacculi. Enzymes were added at various concentrations (see Figs. 4 and
823 S4) and incubated overnight at 37°C. Reactions were then centrifuged for 20 minutes at 16,000g,
824 and the supernatant carefully separated from the pellet. Final values in Figure 4 and S4 are
825 normalized against absorbances measured for reactions with HEWL that were run in tandem for
826 every measurement to correct for differences in different sacculi preparations.

827
828 **Fluorescence microscopy and image preparation.** Fluorescence imaging was done using an
829 inverted Nikon Ti-E microscope using a Plan Apo 60X 1.40 NA oil Ph3 DM objective with a
830 GFP/Cy3 filter cube and an Andor DU885 EM CCD camera. Images were captured using NIS
831 Elements (Nikon). Cells were mounted on 1% (w/v) agarose pads made with PYE (or PBS, in
832 the case of *E. coli*) for imaging. In general, the fluorescent channel of each image was
833 background subtracted and a Gaussian Blur filter was applied using Fiji [81].
834

835 **Western blots.** Strains were grown to saturation (overnight for *C. crescentus* and *A. excentricus*,
836 usually 48 hours for *A. biprosthicum*). OD600 was determined and cells were collected at a
837 normalized density of OD600 = 1/1mL. 1 mL of each normalized culture was pelleted,
838 resuspended in 100 μ L water, and prepared for analysis using standard procedures using SDS-
839 PAGE, transfer, and western blotting. 10 μ L of each sample was loaded onto Any kD Mini-
840 PROTEAN TGX Precast Protein Gels (BioRad). The JL-8 monoclonal GFP antibody (Clontech)
841 was used as the primary antibody and Goat Anti-mouse HRP (Pierce) was used for the secondary
842 antibody. Transferred blots were visualized with SuperSignal West Dura Extended Duration
843 HRP substrate (ThermoFisher Scientific) using a Bio-Rad Chemidoc.
844

845 **Periplasmic expression in *E. coli*.** Fresh Lemo(DE3) competent cells (NEB) were transformed
846 with pET22b constructs containing various muramidase genes with N-terminal H-tags and
847 plated. Lemo21(DE3) carries a rhamnose-inducible copy of LysY that inhibits T7 polymerase
848 and allows for tunable dampening of expression of toxic products. We could not transform
849 expression strains BL21(DE3) or Tuner(DE3) with the pET22b-P22Lyso construct, but were
850 able to isolate a few transformants carrying this construct using Lemo21(DE3) cells under high
851 rhamnose repression (2 mM). P22Lyso-D20L, and all the SpmX-Mur-Cc constructs, efficiently
852 transformed into all expression strains tested, and could be carried by Lemo21(DE3) without
853 rhamnose.

854 In the case of pET22b-P22Lyso, where cells eventually lyse from leak, cell cultures were
855 grown directly from colonies in the presence of 5 mM rhamnose and monitored over time. Figure
856 4A shows the same treatment for all tested constructs. For testing induction of CCM and
857 P22Lyso-D20L, colonies were grown overnight in LB with 100 μ g/mL carbenicillin and 30
858 μ g/mL chloramphenicol. Overnight cultures were diluted 50-fold in LB medium with 100 μ g/mL
859 carbenicillin and 30 μ g/mL chloramphenicol. In experiments cases rhamnose was added at
860 specified concentrations. Typically 4 mL cultures of cells were grown for 1-1.5 hours to an
861 OD600 of 0.3-0.4, induced with 400 μ M IPTG, and shifted to 20°C.

862 *Growth curves and live-dead staining:* Optical densities were measured over time and
863 cells were routinely checked for lysing by microscopy using standard procedures. Briefly, 1 μ L
864 of a 1:1 mixture of solutions A and B from a LIVE/DEAD BacLight Bacterial Viability Kit
865 (ThermoFisher Scientific) was directly added to 100 μ L of cells diluted 1:10 in PBS. Cells were
866 visualized on 1% agar pads made with PBS using the methods described in microscopy.

867 *Periplasmic expression levels:* After growing for 4 h at 20 °C, OD600 was determined
868 and cells were collected at a normalized density of OD600 = 1/1mL. One mL of the normalized
869 sample was pelleted at 4000g for 15 min and the pellet resuspended in 250 μ L 20% sucrose, 1
870 mM EDTA, 30 mM TRIS pH 8 at room temperature. The sample was mixed gently by rotation
871 at room temperature for 10 minutes before being spun down at 13,000g for 10 minutes. The
872 supernatant was carefully removed and the pellet rapidly suspended in 250 μ L ice-cold pure

873 water. The sample was mixed gently by rotation at 4°C for 10 minutes before being spun down
874 at 13,000g at 4°C. The supernatant (periplasmic fraction) and pellet (cell fraction) were then
875 separated and prepared for analysis using standard procedures using SDS-PAGE, transfer, and
876 western blotting. Blots were incubated with His-Probe Antibody (H-3) sc-8136 HRP (Santa Cruz
877 Biotechnology) and visualized with SuperSignal West Dura Extended Duration HRP substrate
878 (ThermoFisher Scientific) using a Bio-Rad Chemidoc.

879

880 **Quantification and Statistical Analysis**

881

882 **HHM logo generation.** WebLogo3 was used to plot the amino acid distribution at each position
883 of the GH motif [52]. To create the alignments for logo generation, 94 T4 lysozyme-like
884 sequences, 20 endolysin/autolysins from the CDD analysis, 60 SpmX muramidase-like
885 sequences (BLAST hits), and 66 SpmX muramidase sequences were simultaneously aligned to
886 T4 lysozyme. See **Table S5** for the genes used in logo construction. Because only sequences
887 with unambiguous alignment in the GH motif were included in this analysis, many
888 endolysin/autolysins from the CDD analysis had to be excluded from the logo. T4 lysozyme-like
889 sequences were chosen from BLAST hits from various bacterial prophage sources.

890

891 **RBB assays.** RBB assays were carried out in triplicate. The averages of the replicates were
892 divided by the average measurement for Hen Egg White Lysozyme (HEWL) activity to obtain
893 the normalized values plotted in the activity curves. The data points plotted in Figure 4A
894 represent measurements of P22-lyso and SpmX-Mur-*Cc* activity over several days. Lines are
895 drawn to help guide the eye toward basic trends and do not reflect line fitting. Data points are
896 from various days and sacculi preparations, but are normalized to parallel reactions with HEWL
897 on the same day and with the same sacculi as each data point.

898

899 **Fluorescent microscopy.** Quantification of stalk morphotypes and stalks with multiple foci was
900 done by hand using tools in Fiji. Quantification of fluorescence data was achieved using
901 MicrobeJ [82]. Mean stalk intensity was measured in *A. biprosthecum* cells by using Fiji to draw
902 line ROIs that did not overlap with the focus at the base of the stalk, measuring mean
903 fluorescence along the ROI. Figures and statistics were performed using GraphPad Prism version
904 8.00 for Mac, GraphPad Software, La Jolla California USA, www.graphpad.com. The statistical
905 details describing the quantification of cell morphology and fluorescent image analysis in Figure
906 S6 can be found in the figure legend.

907

908 **Data and Software Availability**

909 The accession number for the atomic coordinates and structure factors reported in this paper are
910 PDB: 6H9D. The data collection and refinement statistics are summarized in **Table S2**.

911

912 **References**

- 913 1. Hall, J.P.J., Brockhurst, M.A., and Harrison, E. (2017). Sampling the mobile gene pool:
914 innovation via horizontal gene transfer in bacteria. *Phil Trans R Soc B* 372, 20160424.
- 915 2. Koonin, E.V. (2016). Viruses and mobile elements as drivers of evolutionary transitions. *Phil*
916 *Trans R Soc B* 371, 20150442.

- 917 3. Feiner, R., Argov, T., Rabinovich, L., Sigal, N., Borovok, I., and Herskovits, A.A. (2015). A
918 new perspective on lysogeny: prophages as active regulatory switches of bacteria. *Nat. Rev.*
919 *Microbiol.* *13*, 641–650.
- 920 4. Harrison, E., and Brockhurst, M.A. (2017). Ecological and Evolutionary Benefits of
921 Temperate Phage: What Does or Doesn't Kill You Makes You Stronger. *BioEssays* *39*,
922 1700112.
- 923 5. Howard-Varona, C., Hargreaves, K.R., Abedon, S.T., and Sullivan, M.B. (2017). Lysogeny
924 in nature: mechanisms, impact and ecology of temperate phages. *ISME J.* *11*, 1511–1520.
- 925 6. Menouni, R., Hutinet, G., Petit, M.-A., and Ansaldi, M. (2015). Bacterial genome
926 remodeling through bacteriophage recombination. *FEMS Microbiol. Lett.* *362*, 1–10.
- 927 7. Bobay, L.-M., Touchon, M., and Rocha, E.P.C. (2014). Pervasive domestication of defective
928 prophages by bacteria. *Proc. Natl. Acad. Sci.* *111*, 12127–12132.
- 929 8. Touchon, M., Moura de Sousa, J.A., and Rocha, E.P. (2017). Embracing the enemy: the
930 diversification of microbial gene repertoires by phage-mediated horizontal gene transfer.
931 *Curr. Opin. Microbiol.* *38*, 66–73.
- 932 9. Wang, X., Kim, Y., Ma, Q., Hong, S.H., Pokusaeva, K., Sturino, J.M., and Wood, T.K.
933 (2010). Cryptic prophages help bacteria cope with adverse environments. *Nat. Commun.* *1*,
934 147.
- 935 10. Leiman, P.G., Basler, M., Ramagopal, U.A., Bonanno, J.B., Sauder, J.M., Pukatzki, S.,
936 Burley, S.K., Almo, S.C., and Mekalanos, J.J. (2009). Type VI secretion apparatus and
937 phage tail-associated protein complexes share a common evolutionary origin. *Proc. Natl.*
938 *Acad. Sci.* *106*, 4154–4159.
- 939 11. Sarris, P.F., Ladoukakis, E.D., Panopoulos, N.J., and Scoulica, E.V. (2014). A Phage Tail-
940 Derived Element with Wide Distribution among Both Prokaryotic Domains: A Comparative
941 Genomic and Phylogenetic Study. *Genome Biol. Evol.* *6*, 1739–1747.
- 942 12. Ghequire, M.G.K., and De Mot, R. (2015). The Tailocin Tale: Peeling off Phage Tails.
943 *Trends Microbiol.* *23*, 587–590.
- 944 13. Hockett, K.L., Renner, T., and Baltrus, D.A. (2015). Independent Co-Option of a Tailed
945 Bacteriophage into a Killing Complex in *Pseudomonas*. *mBio* *6*, e00452-15.
- 946 14. Scholl, D. (2017). Phage Tail-Like Bacteriocins. *Annu. Rev. Virol.* *4*, 453–467.
- 947 15. Radhakrishnan, S.K., Thanbichler, M., and Viollier, P.H. (2008). The dynamic interplay
948 between a cell fate determinant and a lysozyme homolog drives the asymmetric division
949 cycle of *Caulobacter crescentus*. *Genes Dev.* *22*, 212–225.

- 950 16. Lasker, K., Mann, T.H., and Shapiro, L. (2016). An intracellular compass spatially
951 coordinates cell cycle modules in *Caulobacter crescentus*. *Curr. Opin. Microbiol.* *33*, 131–
952 139.
- 953 17. Jiang, C., Brown, P.J.B., Ducret, A., and Brun, Y.V. (2014). Sequential evolution of bacterial
954 morphology by co-option of a developmental regulator. *Nature* *506*, 489–493.
- 955 18. Perez, A.M., Mann, T.H., Lasker, K., Ahrens, D.G., Eckart, M.R., and Shapiro, L. (2017). A
956 Localized Complex of Two Protein Oligomers Controls the Orientation of Cell Polarity.
957 *mBio* *8*, e02238-16.
- 958 19. Bowman, G.R., Comolli, L.R., Gaietta, G.M., Fero, M., Hong, S.-H., Jones, Y., Lee, J.H.,
959 Downing, K.H., Ellisman, M.H., McAdams, H.H., *et al.* (2010). *Caulobacter* PopZ forms a
960 polar subdomain dictating sequential changes in pole composition and function. *Mol.*
961 *Microbiol.* *76*, 173–189.
- 962 20. Holmes, J.A., Follett, S.E., Wang, H., Meadows, C.P., Varga, K., and Bowman, G.R. (2016).
963 *Caulobacter* PopZ forms an intrinsically disordered hub in organizing bacterial cell poles.
964 *Proc. Natl. Acad. Sci.* *113*, 12490–12495.
- 965 21. Marchler-Bauer, A., Anderson, J.B., Derbyshire, M.K., DeWeese-Scott, C., Gonzales, N.R.,
966 Gwadz, M., Hao, L., He, S., Hurwitz, D.I., Jackson, J.D., *et al.* (2007). CDD: a conserved
967 domain database for interactive domain family analysis. *Nucleic Acids Res.* *35*, D237–D240.
- 968 22. Marchler-Bauer, A., Derbyshire, M.K., Gonzales, N.R., Lu, S., Chitsaz, F., Geer, L.Y., Geer,
969 R.C., He, J., Gwadz, M., Hurwitz, D.I., *et al.* (2015). CDD: NCBI's conserved domain
970 database. *Nucleic Acids Res.* *43*, D222–D226.
- 971 23. Blackburn, N.T., and Clarke, A.J. (2001). Identification of Four Families of Peptidoglycan
972 Lytic Transglycosylases. *J. Mol. Evol.* *52*, 78–84.
- 973 24. Evrard, C., Fastrez, J., and Declercq, J.-P. (1998). Crystal structure of the lysozyme from
974 bacteriophage lambda and its relationship with V and C-type lysozymes I Edited by K.
975 Nagai. *J. Mol. Biol.* *276*, 151–164.
- 976 25. Vollmer, W., Joris, B., Charlier, P., and Foster, S. (2008). Bacterial peptidoglycan (murein)
977 hydrolases. *FEMS Microbiol. Rev.* *32*, 259–286.
- 978 26. Wohlkönig, A., Huet, J., Looze, Y., and Wintjens, R. (2010). Structural Relationships in the
979 Lysozyme Superfamily: Significant Evidence for Glycoside Hydrolase Signature Motifs.
980 *PLOS ONE* *5*, e15388.
- 981 27. Rennell, D., Bouvier, S.E., Hardy, L.W., and Poteete, A.R. (1991). Systematic mutation of
982 bacteriophage T4 lysozyme. *J. Mol. Biol.* *222*, 67–88.
- 983 28. Anand, N.N., Stephen, E.R., and Narang, S.A. (1988). Mutation of active site residues in
984 synthetic T4-lysozyme gene and their effect on lytic activity. *Biochem. Biophys. Res.*
985 *Commun.* *153*, 862–868.

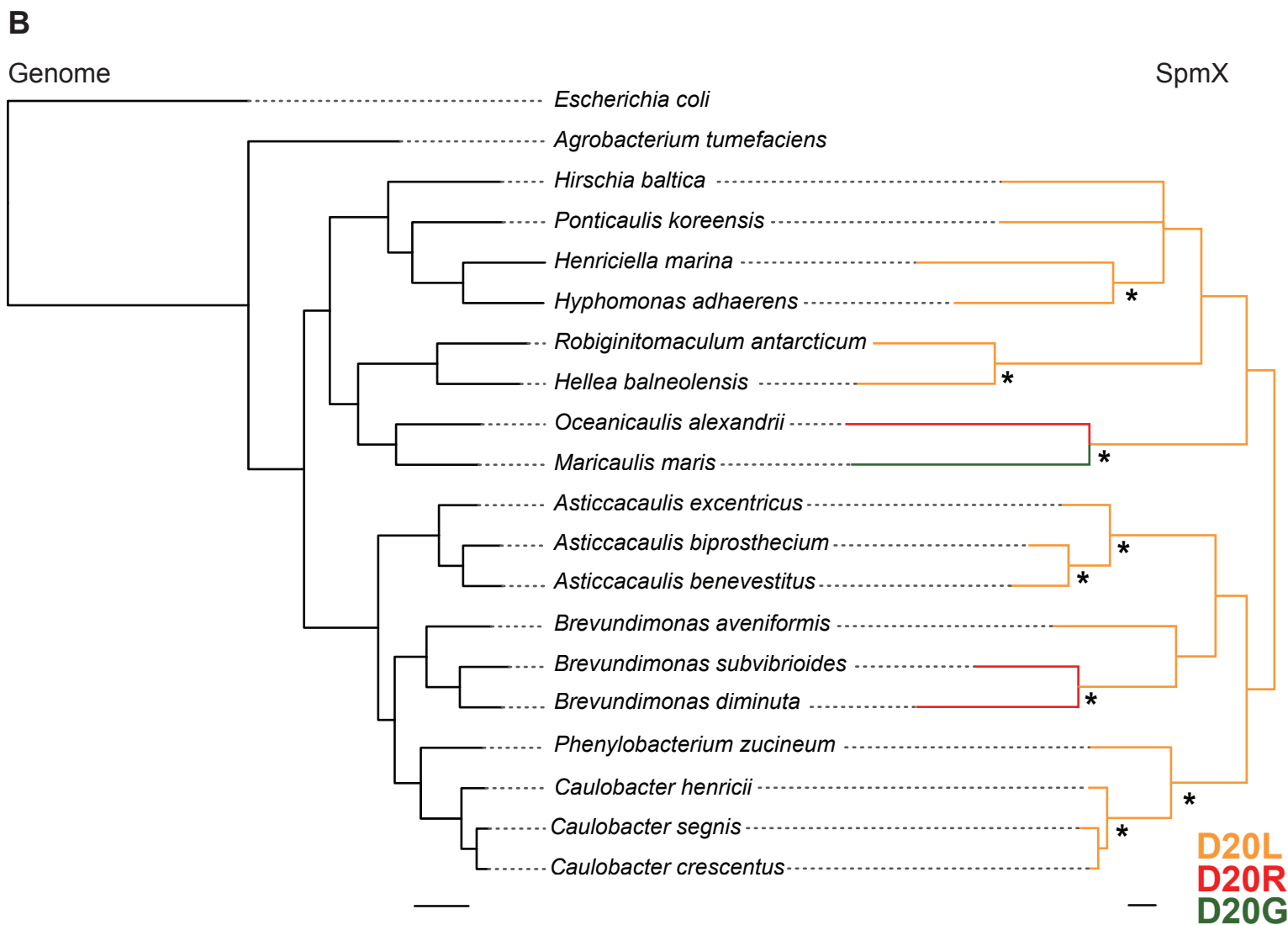
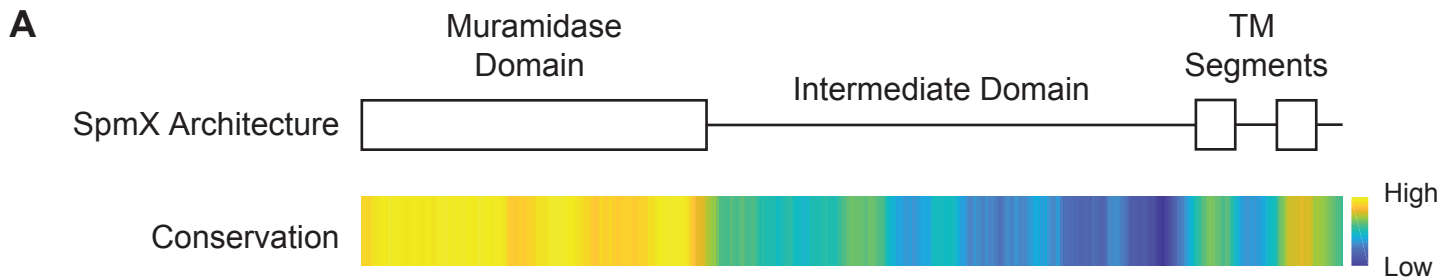
- 986 29. Sun, Q., Kutay, G.F., Arockiasamy, A., Xu, M., Young, R., and Sacchettini, J.C. (2009).
987 Regulation of a muralytic enzyme by dynamic membrane topology. *Nat. Struct. Mol. Biol.*
988 *16*, 1192–1194.
- 989 30. Hardy, L.W., and Poteete, A.R. (1991). Reexamination of the role of Asp20 in catalysis by
990 bacteriophage T4 lysozyme. *Biochemistry* *30*, 9457–9463.
- 991 31. Poteete, A.R., Dao-Pin, S., Nicholson, H., and Mathews, B.W. (1991). Second-site revertants
992 of an inactive T4 lysozyme mutant restore activity by restructuring the active site cleft.
993 *Biochemistry* *30*, 1425–1432.
- 994 32. Anderson, W.F., Grütter, M.G., Remington, S.J., Weaver, L.H., and Matthews, B.W. (1981).
995 Crystallographic determination of the mode of binding of oligosaccharides to T4
996 bacteriophage lysozyme: Implications for the mechanism of catalysis. *J. Mol. Biol.* *147*,
997 523–543.
- 998 33. Braga, L.P.P., Soucy, S.M., Amgarten, D.E., Silva, D., M, A., and Setubal, J.C. (2018).
999 Bacterial Diversification in the Light of the Interactions with Phages: The Genetic Symbionts
1000 and Their Role in Ecological Speciation. *Front. Ecol. Evol.* *6*. Available at:
1001 <https://www.frontiersin.org/articles/10.3389/fevo.2018.00006/full> [Accessed August 30,
1002 2018].
- 1003 34. Canchaya, C., Fournous, G., Chibani-Chennoufi, S., Dillman, M.-L., and Brüßow, H.
1004 (2003). Phage as agents of lateral gene transfer. *Curr. Opin. Microbiol.* *6*, 417–424.
- 1005 35. Cortez, D., Forterre, P., and Gribaldo, S. (2009). A hidden reservoir of integrative elements
1006 is the major source of recently acquired foreign genes and ORFans in archaeal and bacterial
1007 genomes. *Genome Biol.* *10*, R65.
- 1008 36. Daubin, V., and Ochman, H. (2004). Bacterial genomes as new gene homes: the genealogy
1009 of ORFans in *E. coli.*, Bacterial Genomes as New Gene Homes: The Genealogy of ORFans
1010 in *E. coli.* *Genome Res.* *14*, 1036, 1036–1042.
- 1011 37. Brézellec, P., Vallet-Gely, I., Possoz, C., Quevillon-Cheruel, S., and Ferat, J.-L. (2016).
1012 DciA is an ancestral replicative helicase operator essential for bacterial replication initiation.
1013 *Nat. Commun.* *7*, 13271.
- 1014 38. Brézellec, P., Petit, M.-A., Pasek, S., Vallet-Gely, I., Possoz, C., and Ferat, J.-L. (2017).
1015 Domestication of Lambda Phage Genes into a Putative Third Type of Replicative Helicase
1016 Matchmaker. *Genome Biol. Evol.* *9*, 1561–1566.
- 1017 39. Forterre, P. (1999). Displacement of cellular proteins by functional analogues from plasmids
1018 or viruses could explain puzzling phylogenies of many DNA informational proteins. *Mol.*
1019 *Microbiol.* *33*, 457–465.
- 1020 40. Sabehi, G., Shaulov, L., Silver, D.H., Yanai, I., Harel, A., and Lindell, D. (2012). A novel
1021 lineage of myoviruses infecting cyanobacteria is widespread in the oceans. *Proc. Natl. Acad.*
1022 *Sci. U. S. A.* *109*, 2037–2042.

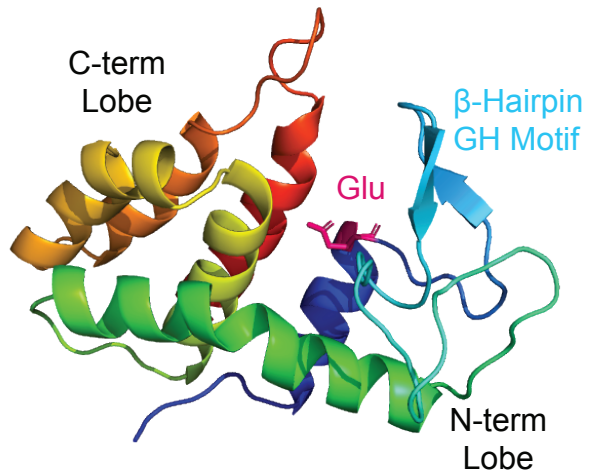
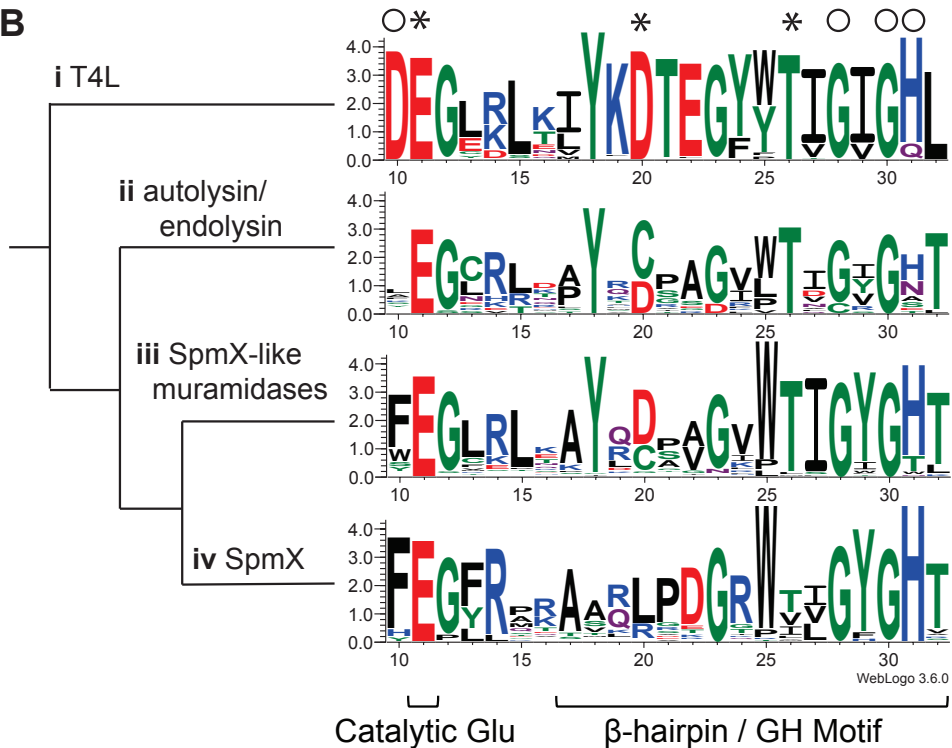
- 1023 41. Lang, A.S., Zhaxybayeva, O., and Beatty, J.T. (2012). Gene transfer agents: phage-like
1024 elements of genetic exchange. *Nat. Rev. Microbiol.* *10*, 472–482.
- 1025 42. Lang, A.S., and Beatty, J.T. (2007). Importance of widespread gene transfer agent genes in
1026 α -proteobacteria. *Trends Microbiol.* *15*, 54–62.
- 1027 43. Shakya, M., Soucy, S.M., and Zhaxybayeva, O. (2017). Insights into origin and evolution of
1028 α -proteobacterial gene transfer agents. *Virus Evol.* *3*. Available at: [https://academic-oup-](https://academic-oup-com.proxyiub.uits.iu.edu/ve/article/3/2/vex036/4705971)
1029 [com.proxyiub.uits.iu.edu/ve/article/3/2/vex036/4705971](https://academic-oup-com.proxyiub.uits.iu.edu/ve/article/3/2/vex036/4705971) [Accessed August 31, 2018].
- 1030 44. Ho, B.T., Dong, T.G., and Mekalanos, J.J. (2014). A View to a Kill: The Bacterial Type VI
1031 Secretion System. *Cell Host Microbe* *15*, 9–21.
- 1032 45. Russell, A.B., Peterson, S.B., and Mougous, J.D. (2014). Type VI secretion system effectors:
1033 poisons with a purpose. *Nat. Rev. Microbiol.* *12*, 137–148.
- 1034 46. Hurst, M.R.H., Glare, T.R., and Jackson, T.A. (2004). Cloning *Serratia entomophila*
1035 Antifeeding Genes—a Putative Defective Prophage Active against the Grass Grub *Costelytra*
1036 *zealandica*. *J. Bacteriol.* *186*, 5116–5128.
- 1037 47. Yang, G., Dowling, A.J., Gerike, U., French-Constant, R.H., and Waterfield, N.R. (2006).
1038 *Photorhabdus* Virulence Cassettes Confer Injectable Insecticidal Activity against the Wax
1039 Moth. *J. Bacteriol.* *188*, 2254–2261.
- 1040 48. Shikuma, N.J., Pilhofer, M., Weiss, G.L., Hadfield, M.G., Jensen, G.J., and Newman, D.K.
1041 (2014). Marine Tubeworm Metamorphosis Induced by Arrays of Bacterial Phage Tail-Like
1042 Structures. *Science* *343*, 529–533.
- 1043 49. Patzer, S.I., Albrecht, R., Braun, V., and Zeth, K. (2012). Structural and Mechanistic Studies
1044 of Pesticin, a Bacterial Homolog of Phage Lysozymes. *J. Biol. Chem.* *287*, 23381–23396.
- 1045 50. Michalska, K., Brown, R.N., Li, H., Jedrzejczak, R., Niemann, G.S., Heffron, F., Cort, J.R.,
1046 Adkins, J.N., Babnigg, G., and Joachimiak, A. (2013). New sub-family of lysozyme-like
1047 proteins shows no catalytic activity: crystallographic and biochemical study of STM3605
1048 protein from *Salmonella Typhimurium*. *J. Struct. Funct. Genomics* *14*, 1–10.
- 1049 51. Ren, Q., Wang, C., Jin, M., Lan, J., Ye, T., Hui, K., Tan, J., Wang, Z., Wyckoff, G.J., Wang,
1050 W., *et al.* (2017). Co-option of bacteriophage lysozyme genes by bivalve genomes. *Open*
1051 *Biol.* *7*, 160285.
- 1052 52. Crooks, G.E., Hon, G., Chandonia, J.-M., and Brenner, S.E. (2004). WebLogo: A Sequence
1053 Logo Generator. *Genome Res.* *14*, 1188–1190.
- 1054 53. Chen, I.-M.A., Markowitz, V.M., Chu, K., Palaniappan, K., Szeto, E., Pillay, M., Ratner, A.,
1055 Huang, J., Andersen, E., Huntemann, M., *et al.* (2017). IMG/M: integrated genome and
1056 metagenome comparative data analysis system. *Nucleic Acids Res.* *45*, D507–D516.

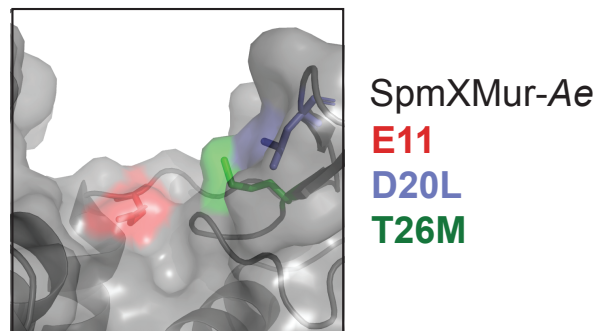
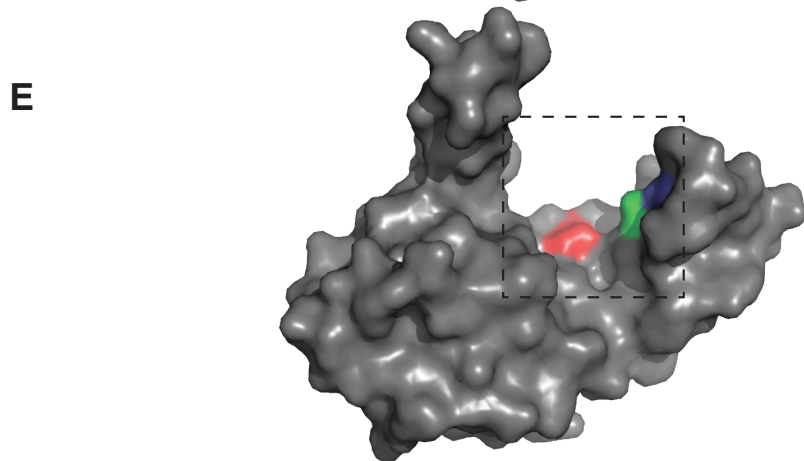
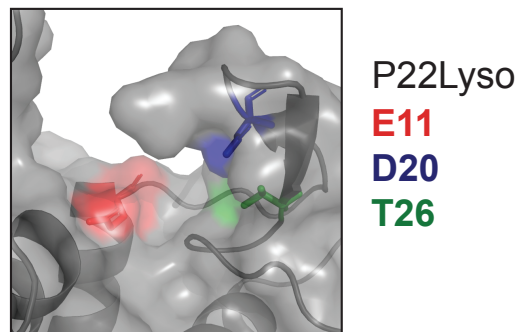
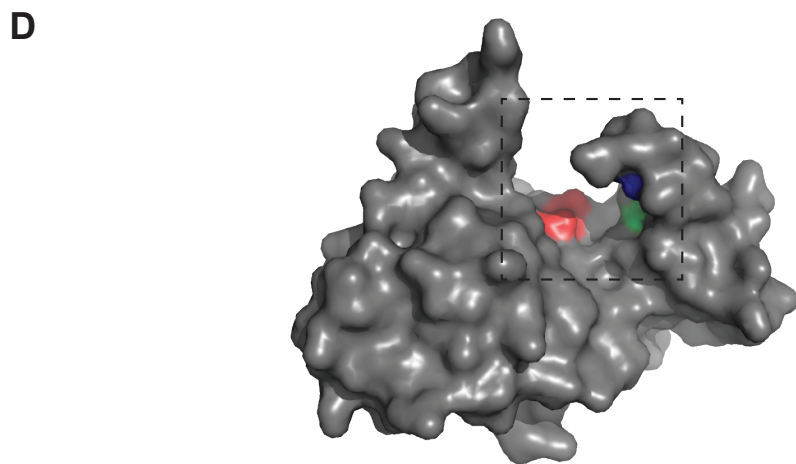
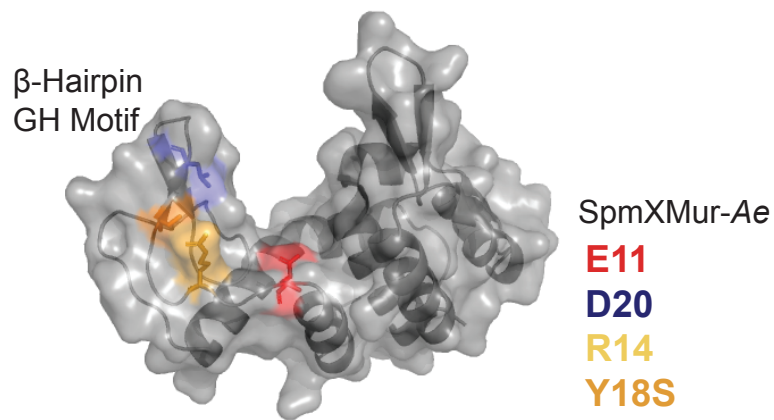
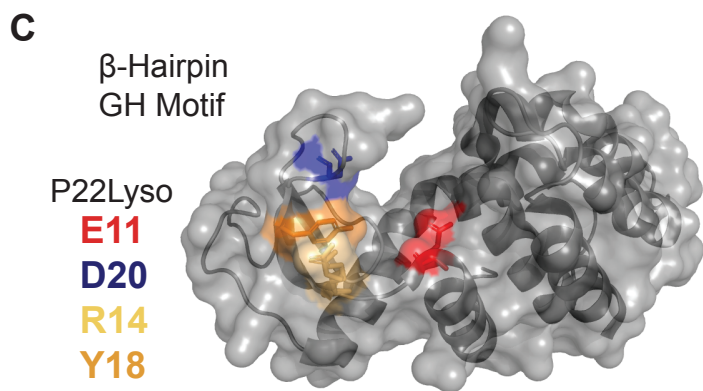
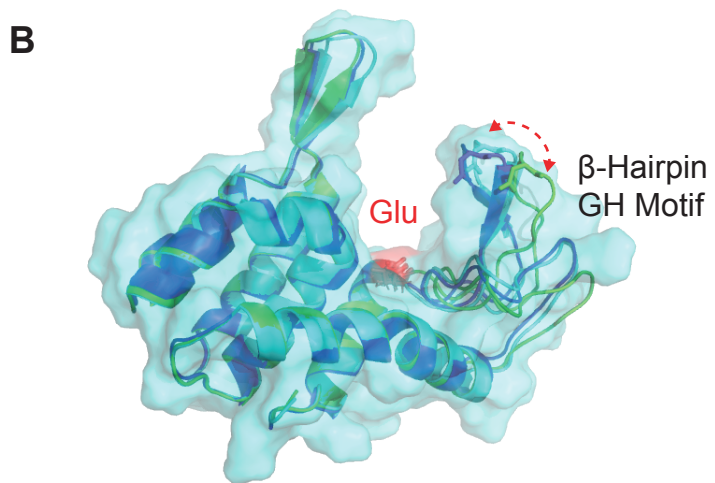
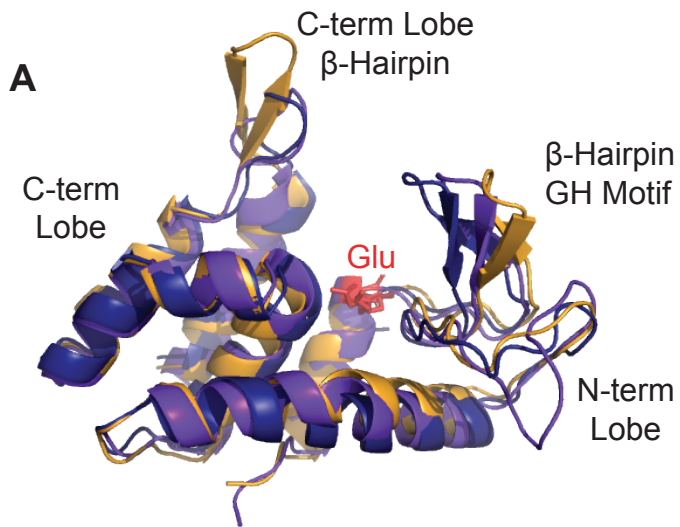
- 1057 54. Edgar, R.C. (2004). MUSCLE: multiple sequence alignment with high accuracy and high
1058 throughput. *Nucleic Acids Res.* *32*, 1792–1797.
- 1059 55. Waterhouse, A.M., Procter, J.B., Martin, D.M.A., Clamp, M., and Barton, G.J. (2009).
1060 Jalview Version 2—a multiple sequence alignment editor and analysis workbench.
1061 *Bioinformatics* *25*, 1189–1191.
- 1062 56. Ashkenazy, H., Erez, E., Martz, E., Pupko, T., and Ben-Tal, N. (2010). ConSurf 2010:
1063 calculating evolutionary conservation in sequence and structure of proteins and nucleic acids.
1064 *Nucleic Acids Res.* *38*, W529–W533.
- 1065 57. Tatusova, T., Ciufu, S., Fedorov, B., O’Neill, K., and Tolstoy, I. (2014). RefSeq microbial
1066 genomes database: new representation and annotation strategy. *Nucleic Acids Res.* *42*,
1067 D553–D559.
- 1068 58. Darling, A.E., Jospin, G., Lowe, E., Iv, F.A.M., Bik, H.M., and Eisen, J.A. (2014). PhyloSift:
1069 phylogenetic analysis of genomes and metagenomes. *PeerJ* *2*, e243.
- 1070 59. Ronquist, F., and Huelsenbeck, J.P. (2003). MrBayes 3: Bayesian phylogenetic inference
1071 under mixed models. *Bioinformatics* *19*, 1572–1574.
- 1072 60. Letunic, I., and Bork, P. (2016). Interactive tree of life (iTOL) v3: an online tool for the
1073 display and annotation of phylogenetic and other trees. *Nucleic Acids Res.* *44*, W242–W245.
- 1074 61. Gonin, M., Quardokus, E.M., O’Donnell, D., Maddock, J., and Brun, Y.V. (2000). Regulation
1075 of Stalk Elongation by Phosphate in *Caulobacter crescentus*. *J. Bacteriol.* *182*, 337–347.
- 1076 62. Thanbichler, M., Iniesta, A.A., and Shapiro, L. (2007). A comprehensive set of plasmids for
1077 vanillate- and xylose-inducible gene expression in *Caulobacter crescentus*. *Nucleic Acids*
1078 *Res.* *35*, e137–e137.
- 1079 63. Figueroa-Cuilan, W., Daniel, J.J., Howell, M., Sulaiman, A., and Brown, P.J.B. (2016).
1080 Mini-Tn7 Insertion in an Artificial attTn7 Site Enables Depletion of the Essential Master
1081 Regulator CtrA in the Phytopathogen *Agrobacterium tumefaciens*. *Appl Env. Microbiol* *82*,
1082 5015–5025.
- 1083 64. Waldo, G.S., Standish, B.M., Berendzen, J., and Terwilliger, T.C. (1999). Rapid protein-
1084 folding assay using green fluorescent protein. *Nat. Biotechnol.* *17*, 691–695.
- 1085 65. Marblestone, J.G., Edavettal, S.C., Lim, Y., Lim, P., Zuo, X., and Butt, T.R. (2006).
1086 Comparison of SUMO fusion technology with traditional gene fusion systems: enhanced
1087 expression and solubility with SUMO. *Protein Sci. Publ. Protein Soc.* *15*, 182–189.
- 1088 66. Uehara, T., Parzych, K.R., Dinh, T., and Bernhardt, T.G. (2010). Daughter cell separation is
1089 controlled by cytokinetic ring-activated cell wall hydrolysis. *EMBO J.* *29*, 1412–1422.
- 1090 67. Bowler, M.W., Nurizzo, D., Barrett, R., Beteva, A., Bodin, M., Caserotto, H., Delagenière,
1091 S., Dobias, F., Flot, D., Giraud, T., *et al.* (2015). MASSIF-1: a beamline dedicated to the

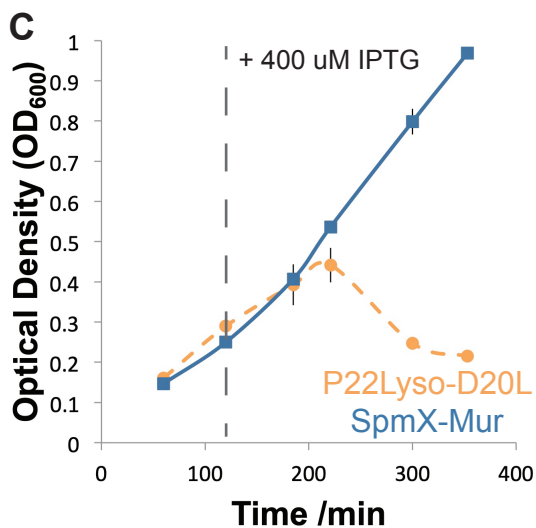
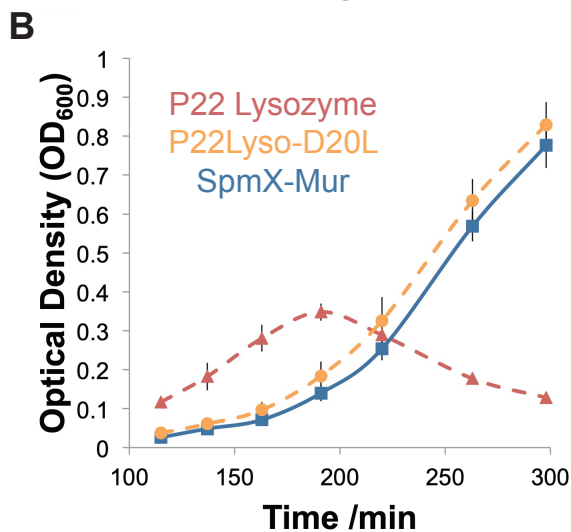
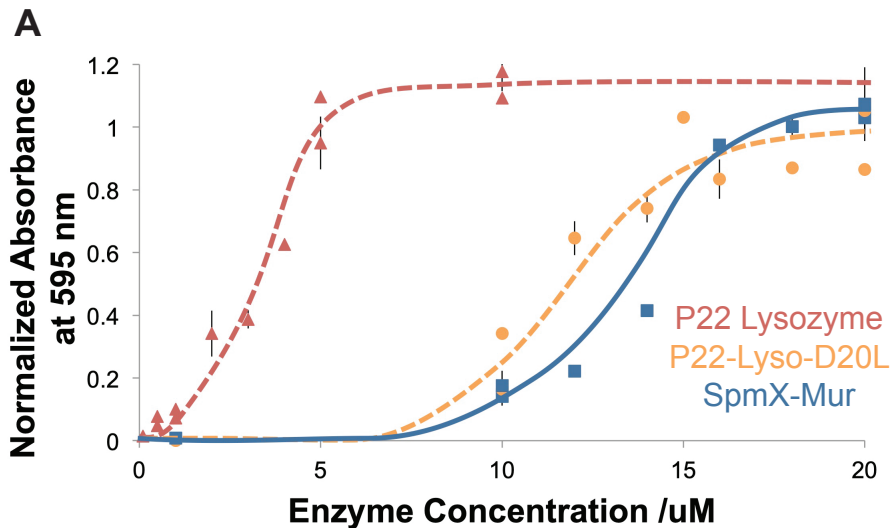
- 1092 fully automatic characterization and data collection from crystals of biological
1093 macromolecules. *J. Synchrotron Radiat.* *22*, 1540–1547.
- 1094 68. Svensson, O., Malbet-Monaco, S., Popov, A., Nurizzo, D., and Bowler, M.W. (2015). Fully
1095 automatic characterization and data collection from crystals of biological macromolecules.
1096 *Acta Crystallogr. D Biol. Crystallogr.* *71*, 1757–1767.
- 1097 69. Kabsch, W. (2010). XDS. *Acta Crystallogr. D Biol. Crystallogr.* *66*, 125–132.
- 1098 70. McCoy, A.J., Grosse-Kunstleve, R.W., Adams, P.D., Winn, M.D., Storoni, L.C., and Read,
1099 R.J. (2007). Phaser crystallographic software. *J. Appl. Crystallogr.* *40*, 658–674.
- 1100 71. Terwilliger, T.C., Grosse-Kunstleve, R.W., Afonine, P.V., Moriarty, N.W., Zwart, P.H.,
1101 Hung, L.-W., Read, R.J., and Adams, P.D. (2008). Iterative model building, structure
1102 refinement and density modification with the PHENIX AutoBuild wizard. *Acta Crystallogr.*
1103 *D Biol. Crystallogr.* *64*, 61–69.
- 1104 72. Emsley, P., and Cowtan, K. (2004). Coot: model-building tools for molecular graphics. *Acta*
1105 *Crystallogr. D Biol. Crystallogr.* *60*, 2126–2132.
- 1106 73. Langer, G.G., Cohen, S.X., Lamzin, V.S., and Perrakis, A. (2008). Automated
1107 macromolecular model building for X-ray crystallography using ARP/wARP version 7. *Nat.*
1108 *Protoc.* *3*, 1171–1179.
- 1109 74. Murshudov, G.N., Skubák, P., Lebedev, A.A., Pannu, N.S., Steiner, R.A., Nicholls, R.A.,
1110 Winn, M.D., Long, F., and Vagin, A.A. (2011). REFMAC5 for the refinement of
1111 macromolecular crystal structures. *Acta Crystallogr. D Biol. Crystallogr.* *67*, 355–367.
- 1112 75. Brünger, A.T. (1992). Free R value: a novel statistical quantity for assessing the accuracy of
1113 crystal structures. *Nature* *355*, 472–475.
- 1114 76. Laskowski, R.A., MacArthur, M.W., Moss, D.S., and Thornton, J.M. (1993). PROCHECK: a
1115 program to check the stereochemical quality of protein structures. *J Appl Crystallogr.* 283–
1116 291.
- 1117 77. Kabsch, W., and Sander, C. (1983). Dictionary of protein secondary structure: pattern
1118 recognition of hydrogen-bonded and geometrical features. *Biopolymers* *22*, 2577–2637.
- 1119 78. Hayashi, K. (1975). A rapid determination of sodium dodecyl sulfate with methylene blue.
1120 *Anal. Biochem.* *67*, 503–506.
- 1121 79. Uehara, T., Parzych, K.R., Dinh, T., and Bernhardt, T.G. (2010). Daughter cell separation is
1122 controlled by cytokinetic ring-activated cell wall hydrolysis. *EMBO J.* *29*, 1412–1422.
- 1123 80. Zhou, R., Chen, S., and Recsei, P. (1988). A dye release assay for determination of
1124 lysostaphin activity. *Anal. Biochem.* *171*, 141–144.

- 1125 81. Schindelin, J., Arganda-Carreras, I., Frise, E., Kaynig, V., Longair, M., Pietzsch, T.,
1126 Preibisch, S., Rueden, C., Saalfeld, S., Schmid, B., *et al.* (2012). Fiji: an open-source
1127 platform for biological-image analysis. *Nat. Methods* 9, 676–682.
- 1128 82. Ducret, A., Quardokus, E.M., and Brun, Y.V. (2016). MicrobeJ, a tool for high throughput
1129 bacterial cell detection and quantitative analysis. *Nat. Microbiol.* 1, 16077.
- 1130 83. Evinger, M., and Agabian, N. (1977). Envelope-associated nucleoid from *Caulobacter*
1131 *crenscentus* stalked and swarmer cells. *J. Bacteriol.* 132, 294–301.
- 1132
1133 84. Poindexter, J.S. (1964). BIOLOGICAL PROPERTIES AND CLASSIFICATION OF THE
1134 CAULOBACTER GROUP1. *Bacteriol. Rev.* 28, 231–295.
- 1135
1136 85. Pate, J.L., and Ordal, E.J. (1965). THE FINE STRUCTURE OF TWO UNUSUAL
1137 STALKED BACTERIA. *J. Cell Biol.* 27, 133–150.
- 1138
1139 86. Mooers, B.H.M., and Matthews, B.W. (2006). Extension to 2268 atoms of direct methods in
1140 the ab initio determination of the unknown structure of bacteriophage P22 lysozyme. *Acta*
1141 *Crystallogr. D Biol. Crystallogr.* 62, 165–176.
- 1142
1143 87. Meisner, J., Llopis, P.M., Sham, L.-T., Garner, E., Bernhardt, T.G., and Rudner, D.Z. (2013).
1144 FtsEX is required for Cw10 peptidoglycan hydrolase activity during cell wall elongation in
1145 *Bacillus subtilis*. *Mol. Microbiol.* 89, 1069–1083.
- 1146
1147

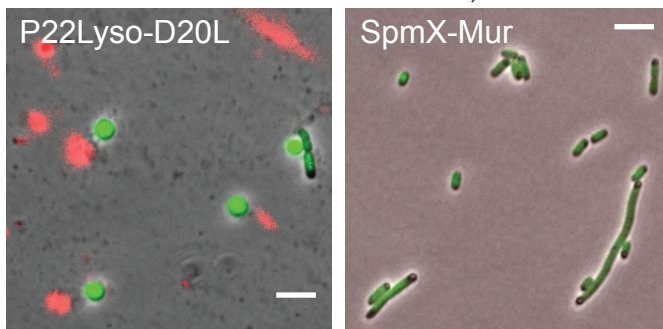


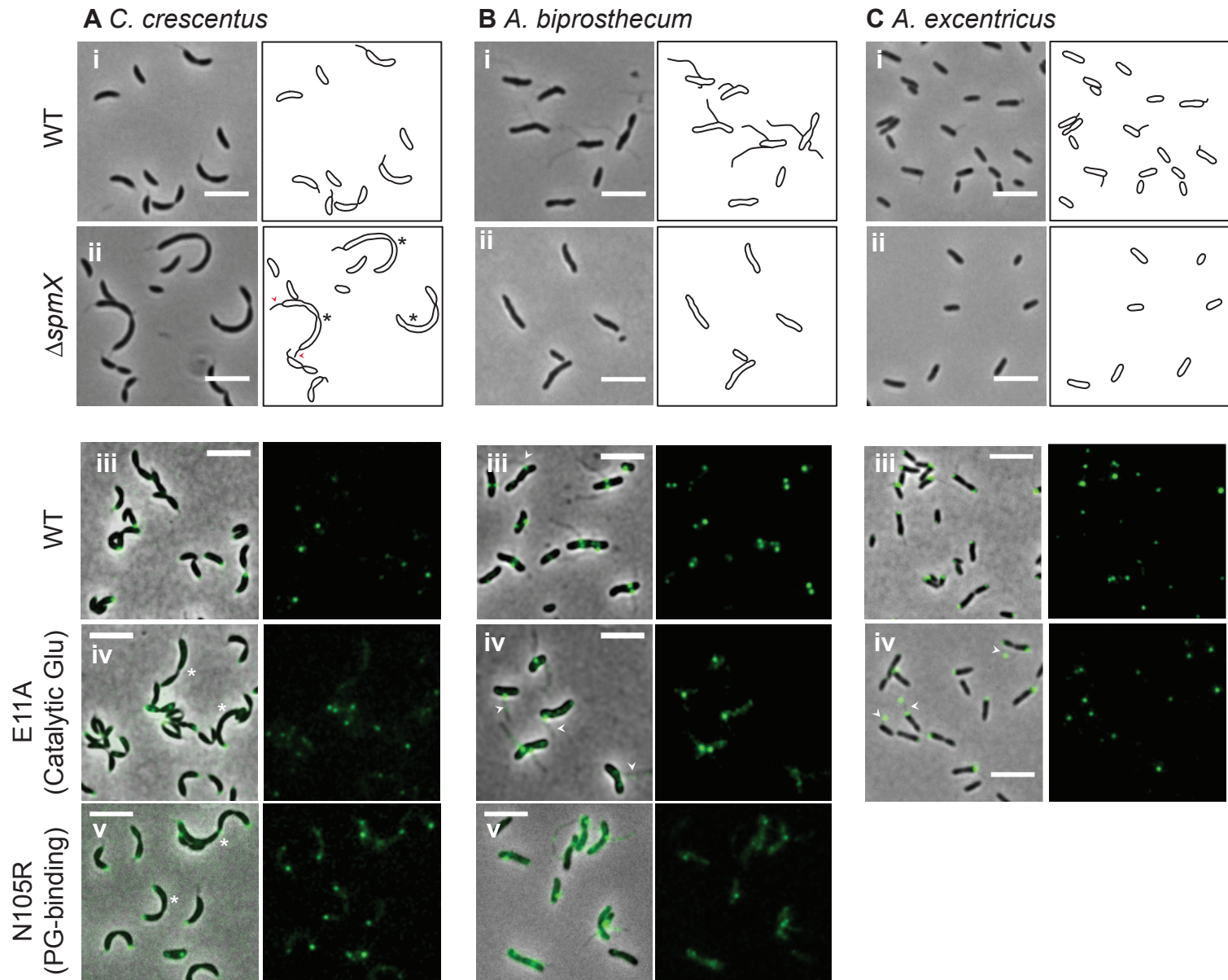
A**B**

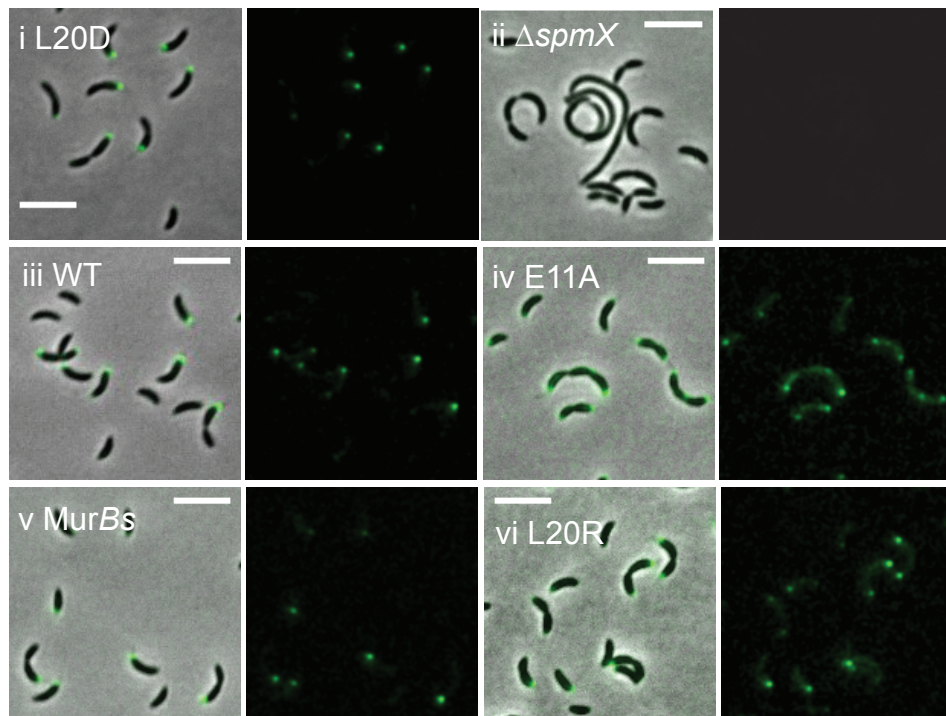
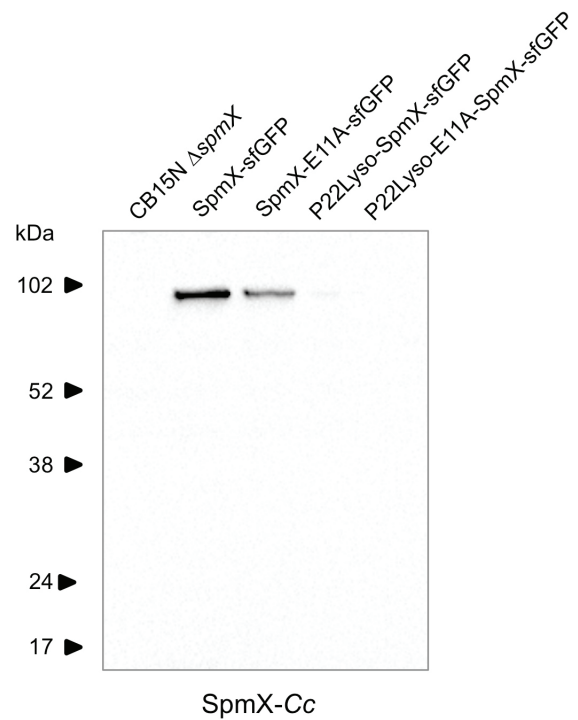


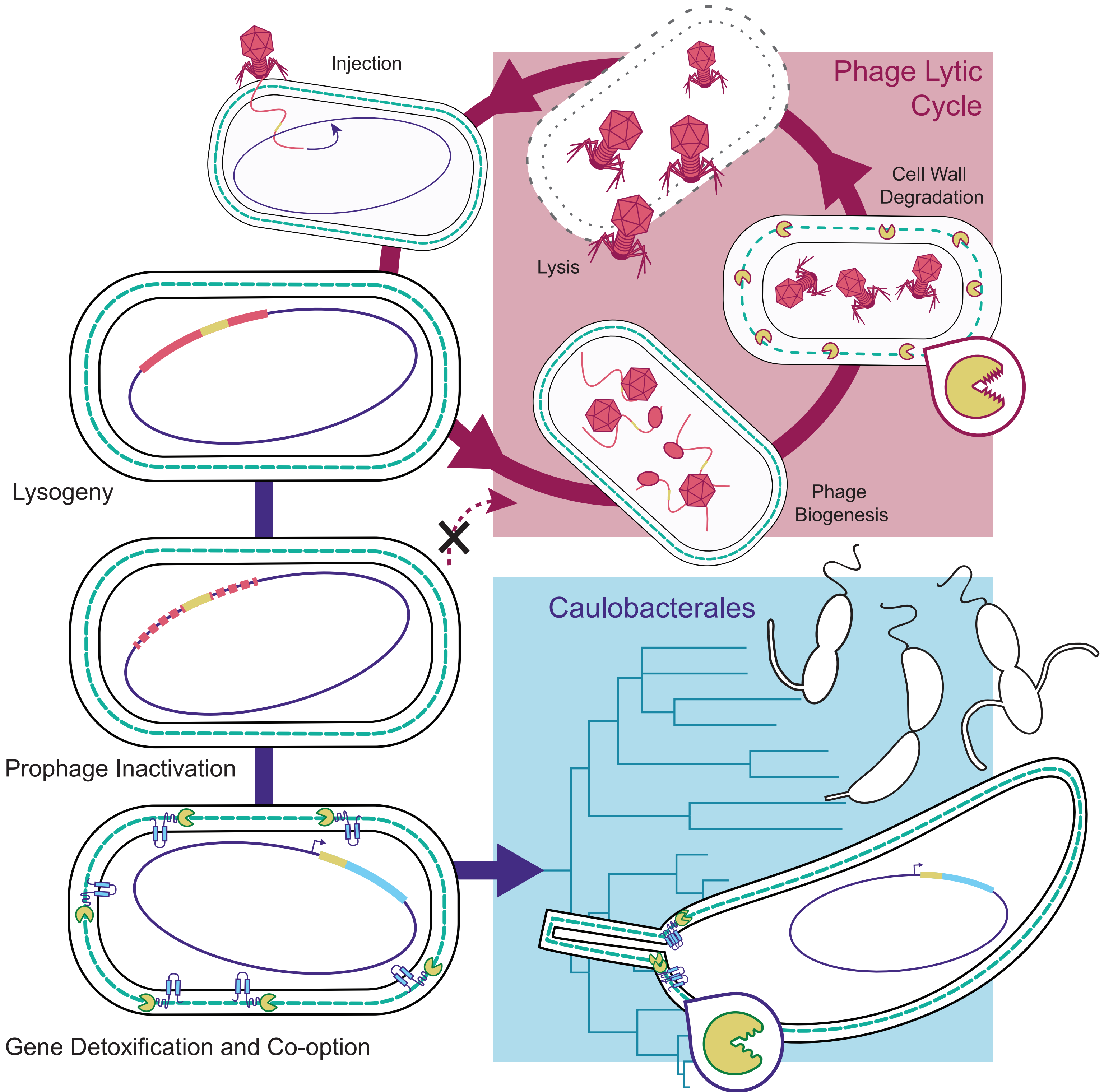


D Live-Dead Stain:
 SYTO9: live cells / PI: dead cells, free DNA





A**B**



Lysogeny

Prophage Inactivation

Gene Detoxification and Co-option

Caulobacterales

